Pure

Scotland's Rural College

Emerging two-dimensional (2D) MXene-based nanostructured materials

Wang, Rui; Young Jang, Won; Zhang, Wen; Venkata Reddy, Ch; Kakarla, Raghava Reddy; Li, Changping; Gupta, Vijai Kumar; Shim, Jaesool; Aminabhavi, Tejraj M.

Link to publication

Emerging two-dimensional (2D) MXene-based nanostructured materials: Synthesis strategies, properties, and applications as efficient pseudo-supercapacitors

Rui Wang [a], Won Young Jang [a], Wen Zhang [a], Ch. Venkata Reddy [a,*], Raghava Reddy Kakarla [b,*], Changping Li [c], Vijai Kumar Gupta [d], Jaesool Shim [a,*], Tejraj M. Aminabhavi [e,*]

[a] School of Mechanical Engineering, Yeungnam University, Gyeongsan 712-749, Republic of Korea
[b] School of Chemical and Biomolecular Engineering, The University of Sydney, Sydney, NSW 2006, Australia
[c] College of Mechanical and Electrical Engineering, Hunan University of Science and Technology, Xiangtan 411201, China
[d] Biorefining and Advanced Materials Research Centre, SRUC, Barony Campus, Parkgate, Dumfries DG1 3NE, United Kingdom
[e] Center for Energy and Environment, School of Advanced Sciences, KLE Technological University, Hubballi 580031, India

ARTICLE INFO

ABSTRACT

Supercapacitors, which are essential for addressing modern energy challenges, possess outstanding energy storage capabilities without requiring manual maintenance. However, their low energy density and capacity limit their applicability for electrode materials. Recently, two-dimensional materials (2D), and particularly 2D transition metal carbonitrides (MXenes) have attracted considerable interest for developing energy storage devices because of their large specific surface area and fast ion-transport pathways. MXenes mainly comprise a transition metal (M) layer, carbon and/or nitrogen (X) layer, and active functional groups exterior to the layer. Metallic properties of the M layer offer excellent pseudocapacitance characteristics, while X layer is characterized by abundant active sites and conductivity similar to that of graphene. Compared with conventional materials, the existence of various functional groups on the surface of MXenes endows them with stronger hydrophilicity and higher wettability in aqueous electrolytes, which, combined with their diverse frame structures and functional group combinations, significantly augment their applicability for energy storage devices. Therefore, it is necessary to summarize and analyze the research results on MXenses. This review addresses the applications of MXenes in energy storage supercapacitors along with current challenges and solutions including intercalation, doping, surface modification methods, and heterogeneous structures. Finally, the prominent contemporary research trends are comparatively discussed to promote research and development in this field in the near future.

1. Introduction

The present world is experiencing an unprecedented energy crisis. Economic development in the past few decades has been highly dependent on limited fossil fuels [1]. The depletion of oil resources, accumulation of greenhouse gases, abnormal climate, and environmental pollution have posed a threat to human survival [2–5]. Therefore, developing a green economy that efficiently utilizes renewable resources is a viable way to sustain human civilization. Currently, renewable resources, such as solar energy, wind energy, and photovoltaic power, manage to alleviate the pressure of energy shortage to a certain extent [6]. However, the constant availability of such energy sources is naturally limited, which is difficult to control, thereby highlighting the need for efficient energy-storage media to accommodate the needs of modern society [7]. Supercapacitors occupy a dominant position in the energy storage field, owing to their high power density, super cycle-life, and non-requirement of manual maintenance. These characteristics render them highly suitable for green and sustainable development, and thus crucial for addressing the energy crisis [8].

Energy storage mechanism classifies supercapacitors into electric double-layer capacitors (EDLCs) and pseudocapacitors. The energy storage mechanism of EDLCs relies purely on physical electrostatic

adsorption; therefore, energy storage performance is highly dependent on specific surface area (SSA) of the electrode materials [9]. In contrast, the energy storage mechanism of pseudocapacitors is based on reversible electrochemical reactions (redox reactions) that occur on the electrode material's surface, and help achieve a higher specific capacitance and energy density than the traditional EDLCs. Although pseudocapacitors represent the future development trend of supercapacitors, their energy storage characteristics involve multiple caveats such as the SSA, number of active sites, and redox functional groups of the materials. Therefore, the development of pseudocapacitors is directly related to the efficiency of the electrode materials.

Recently, 2D materials, and especially MXenes, have attracted considerable attention for their applications in supercapacitors due to their high specific surface area and short ion transport pathways. The 2D transition metal carbides and carbonitrides, an emerging family of materials called Mxenes, were pioneered by Gogotsi et al. [10]. In addition to their traditional 2D material properties, these also possess unique physical and electrochemical properties. Moreover, their varied layered structures, transition metal frameworks, and extra-layer functional groups endow them with numerous unexplored possibilities [11]. MXenes-based adsorbent materials have also found potential applications in the realm of electronic waste (e-waste) and mineral treatment due to their capacity for metal (e.g., Au, Ag, etc.) adsorption from both ore and e-waste sources. Similar to graphene structure, their discovery has kickstarted a wave of research endeavors that expands over many fields, including batteries, supercapacitors, and photocatalysis, with related reports that have increased exponentially in just ten years (Fig. 1). Despite having already been reviewed by many scholars, the logical relationship between the material structure of MXene and its physical properties remains unclear [12–15]. Also, owing to their significantly different storage mechanisms, approaching different storage mechanisms such as batteries, EDLCs, and pseudocapacitors, from a common scientific standpoint is almost impossible [16–18].

Majority of findings mainly focus on studies conducted before 2017, suggesting that few researchers have summarized and analyzed the explosive growth in recent years for pseudocapacitors with higher energy density (the best commercial EDLCs only reach ~ 10 Wh/kg) and their application prospects [12,19]. Given the large number of related publications, it is significant to promote the development of new MXenes for applications in pseudocapacitors as novel energy sources to systematically address the current energy crisis.

In this review, we discuss and analyze the latest research results on the use of MXenes in the field of pseudocapacitors to better clarify the logical relationship between their material structure and mechanism of pseudocapacitive storage from the prospects of surface functional groups, spatial design, and effect of elemental content on electrochemical performance. From the birth, development, technical difficulties, and prospects of MXene materials, their application path in pseudocapacitors is discussed. Current technical problems and material modification methods are introduced, which will provide valuable insight for more profound application research. This article's basic knowledge encourages new researchers to enter the field of MXene-based pseudocapacitors. The more advanced parts of this review stimulate researchers to generate more novel ideas and promote their applications in the energy storage field.

2. Family of MXenes

2.1. Origin of MXene

MXene is novel 2D material invented in 2011 and developed into a family of materials in just a few years. It is a general term for transition metal carbides (TMC) and transition metal nitrides (TMN) formed by the selective etching of MAX phase precursors [20]. The origin of this name is closely related to the MAX precursor. MAX is a ceramic material (such as Ti_3SiC_2 and Ti_2AlC), where M represents the transition metal, A is the main group element, and X is carbon and/or nitrogen [21]. The atomic layers of MAX are mainly connected by van der Waals forces, of which the force between layers A and MX is weak; therefore, layer A is easily etched away to form the MX material. After the etching process, 2D sheet structure with graphite-like physical and electrochemical properties is formed, known as MXene (pronounced MXene) [10]. It is also worth mentioning that in the exfoliation process of the main group element layer under different environments, various functional groups (-F, –OH, and -O) with different distributions are often introduced to the surface of MXene. The complete MXene material can be regarded as consisting of a transition metal layer (M), carbon–nitrogen layer (X), and termination layer (T); therefore, its general chemical formula can be expressed as $M_{n+1}X_nT_x$ (n = 1–4). After different combinations and calculations of the M−layer and X-layer elements, many scholars have
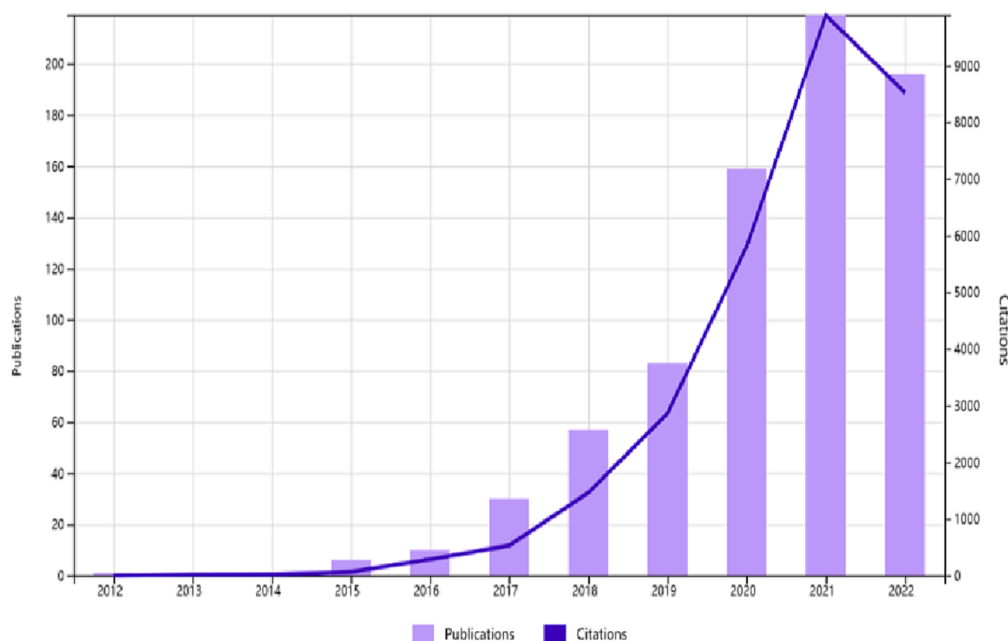

Fig. 1. Trend in the number of citations and publications related to MXenes and its numerous uses according to the data from the Web of Science.

predicted and synthesized multiple MXenes. In 2015, Anasori et al. [22] calculated and predicted more than 25 ordered MXenes using density functional theory (DFT). Subsequently, in 2017, Anasori et al. [23] predicted more than 40 different MXene types and pointed out that more than 20 have been synthesized at that stage. Recently, in 2019, Gogotsi et al. [11] reported at least 100 stoichiometric combinations of MXenes. Overall, the MXene family has expanded exponentially over the past few years, demonstrating its remarkable versatility.

Generally, different MAX precursors can be selectively exfoliated from layer A to obtain specific MXene systems, which are mainly divided into M_2XT_x, $M_3X_2T_x$, and $M_4X_3T_x$. Fig. 2a. [24] shows the preparation process, that is, the selective A layer-etching process [24]. Each family contains several MXene materials: for example, the M_2XT_x type includes Ti_2CT_x [25,26], Mo_2CT_x [27,28], Nb_2CT_x [29], and Hf_2CT_x [30]. The $M_3X_2T_x$ type includes $Ti_3C_2T_x$ [31–33], $Cr_3C_2T_x$ [34], and $Hf_3C_2T_x$ [35], and the $M_4X_3T_x$ contains $Nb_4C_3T_x$ [36], $Ti_4N_3T_x$ [37], etc. Fig. 2b [20] illustrates the selective exfoliation process of different MAXs to obtain specific MXene types, where M_2AX, M_3AX_2, and M_4AX_3 cover all kinds (211 phase, 312 phase, and 413 phase) of MAX phase. The classification of these phases depends on the value of n in the general formula $M_{n+1}AX_n$. Until this point, more than 70 MAX phases have been found

[38]. From this, it can be undoubtedly inferred that the structure of the precursor MAX plays a pivotal role in determining the MXene type. However, some researchers have used non-MAX materials instead of traditional precursor sources and have successfully prepared MXenes with the same properties. Meshkian et al. [39] prepared 2D Mo_2CT_x using a gallium-based atomic laminate Mo_2Ga_2C (double A-layer phase) under hydrofluoric acid etching. Correspondingly, Zhou et al. [40] synthesized Hf-containing MXenes by following a selective exfoliation process and using a $Hf_3[Al(Si)]_4C_6$ (non-MAX phase) compound as the precursor. Although these materials are prepared via the exfoliation of the MAX-like phase rather than MAX precursors, such as solid solution double M−layer, ordered double M−layer and ordered divacancy MAX-like phase [11,38,41], they are all 2D transition metal carbonitrides in nature; hence, they also belong to the MXene material family. To obtain MXenes with higher energy storage performance, many scholars have conducted research on multi-transition metal (bimetal or above) MXenes [42]. Therefore, MXene is classified as 2D product formed by the selective exfoliation of MAX materials. However, it is necessary to pay attention to whether the structure of the material satisfies the framework of the MXene system, because its frame structure is of paramount importance in determining its pseudocapacitive
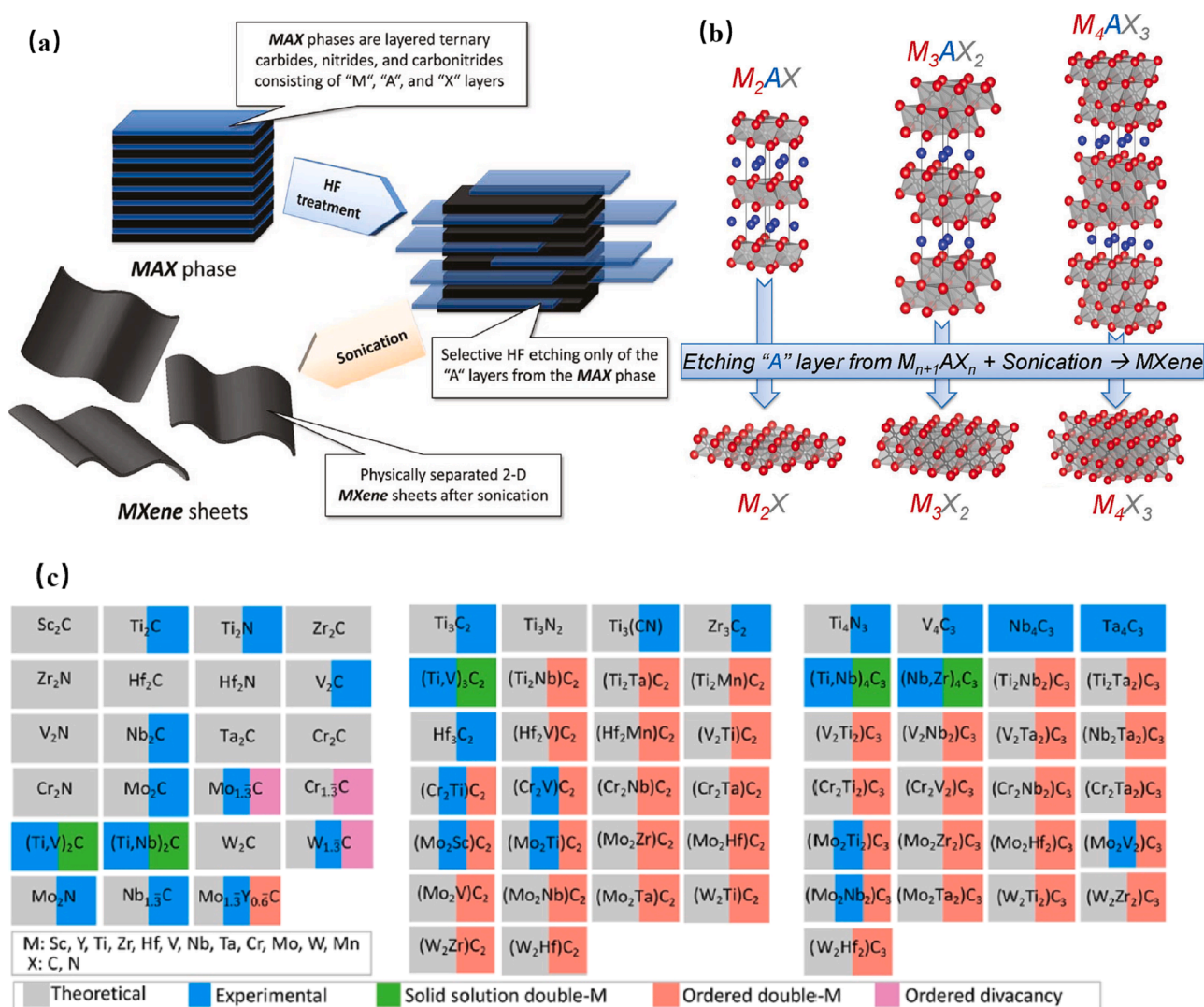
Fig. 2. (a) Preparation principle of MXene: selective exfoliation etching by MAX phase. Reproduced with permission from Ref. [24] Copyright 2012, American Chemical Society. (b) The process of generating different types of MXenes. Reproduced with permission from Ref. [20] Copyright 2014, Wiley-Blackwell. (c) MXene species that have been practically synthesized or theoretically formed at present. Reproduced with permission from Ref. [11] Copyright 2019, American Chemical Society.

performance.

All possible chemical formulas of MXene materials that can be obtained after the removal of the A layer can be calculated based on the precursor MAX phase species that are currently known. Fig. 2c [11] shows the most promising MXene types that have been practically synthesized, or theoretically formed at the current stage because currently, it is not feasible to extract these MXene materials by exfoliating the too excessively robust metal bond of layer A since this process remains a challenge (Specifically, it will be discussed in detail in section 3 of Synthesis.). Altogether, their families will become more prominent with further research.

2.2. Structure and properties of MXene

The family line refers to the general name of a class of substances with similar structures and properties. MXene is a hexagonal crystal system that belongs to the P6$_3$/mmc space group, identical to MAX. In the MAX phase, the M (transition metal) and X (carbon–nitrogen) atoms are covalently linked to form the M$_6$X octahedron, where the X atom is located in the octahedral center. The M atoms are hexagonal close-packed (hcp), whereas the A atoms are staggered between the space group and the gap. Compared with M and X atoms, A atoms are more active, have weaker bond energy, and are easier to chemically remove by etching. During the selective peel-off of the A layer, the M−X covalent bond remains intact. Still, new miscellaneous terminations (–OH, -O, -F, etc.) are formed, and the original area space of the A atomic layer is squeezed. After further compression, the whole material forms a 2D layered structure [41,42]. Consequently, MXene is mainly composed of M, X, and T functional groups outside the layer, which is a compressed 2D layered structure. At present, the first approach discussed above constitutes the conventional research methodology on the structure of MXenes. However, it ignores the influence of surface defects and assumes that the T functional terminations outside the layer are uniformly distributed [45].

Microscopically, MXene is generally shaped like a multilayer accordion (Fig. 3a. [46]), where strong van der Waals forces keep the layers interlinked. The abundant terminations on the outer surface endow the material with extreme hydrophilicity, comparable to that of graphene oxide [45,46]. It is worth noting that MXene surface functional groups are both hydrophilic and conductive, which is not common in 2D materials. For example, the termination on the surface of graphene significantly reduces its conductivity, although it is hydrophilic. Therefore, various researchers have been developing high-purity reduced graphene oxide (rGO) to control the presence of functional groups [47,48]. However, the surface terminations of MXene do not significantly reduce

the electrical conductivity of the material. And its storage performance is largely attributed to its external functional groups, which offer limitless possibilities for tuning. Therefore, compared to other conventional 2D materials, MXene allows for more extensive and controllable adjustments. In contrast, the rich and varied structure and distribution of the surface functional groups offer many modification possibilities, which is a current research hotspot.

First-principles and experimental studies have shown that the energy storage performance of MXene is closely related to its miscellaneous groups (Fig. 3b, 3c, and 3d) [51]. Feng et al. [52] highlighted that the -F and –OH surface groups exacerbate the difficulty of delamination during the selective etching process, which, apart from increasing the preparation time of MXene, may also cause a stacking effect. Zhan et al. [53] pointed out that the surface -H terminations can influence the point of zero charges (PZC) in MXenes, which affects their pseudocapacitive properties. Subsequently, Mu et al. [54] observed via in situ X-ray absorption spectroscopy that -O terminations actively participate in the pseudocapacitive reactions, which is conducive for enhancing the pseudocapacitive performance. Overall, by merely changing their outer terminal groups, MXenes can be designed to accomplish different functionalities, showing their versatility for energy storage applications.

Further, the multiple transition metal particles existing in the M layer on the MXene surface endow it with pseudocapacitive properties, owing to the reversible electrochemical reactions of the transition metal multivalent states. Accordingly, the transition metal element is the most critical factor in determining the pseudocapacitive performance, and the design of MXenes using multicomponent composite metals is of great significance [55]. Although the transition-metal layer increases the pseudocapacitance of the material in terms of energy storage, it also increases its chemical activity, making it more susceptible to ambient temperature and humidity. When the material is warm and moist, it is easily oxidized or decomposed into metal oxides and carbon [54,55]. The entire oxidative decomposition process is mainly caused by the gradual spread of metal oxide crystals from the edge to the center of the 2D layered structure through nucleation and growth. The initial oxidation of MXene reduces the number of active energy storage sites on the material surface. In contrast, further oxidation leads to the decomposition of the entire MXene and the complete loss of its performance. Zhang et al. [58] compared the morphologies of MXenes at the initial stages of preparation and storage in air for 7 and 30 d, and discovered that their color gradually became lighter under extended air exposure till it finally turned transparent. SEM observations revealed that the oxidative decomposition process started from the edge of the material and gradually spread to the center (Fig. 3e, f, and g [58]). Moreover, the performance of the oxidized MXenes progressively decreased, showing
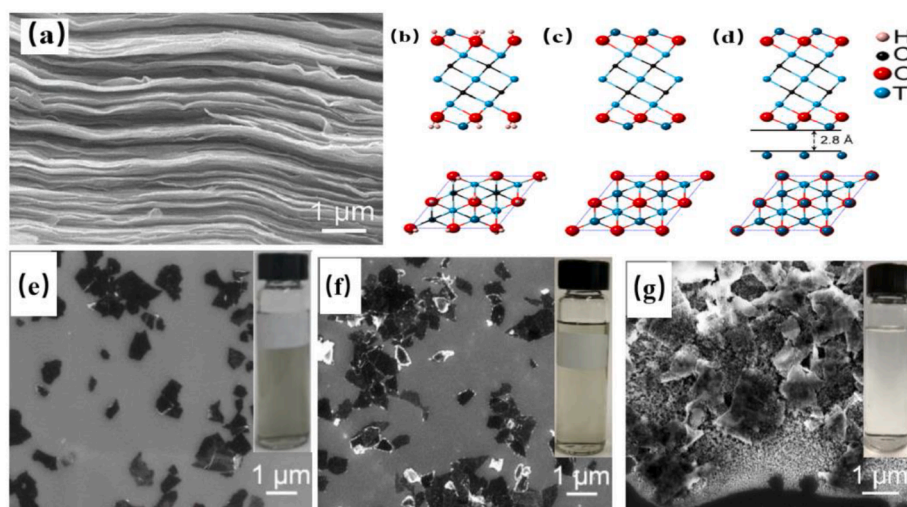
Fig. 3. (a) Cross-sectional SEM image of Ti$_3$C$_2$ showing its typical layered accordion shape. Reproduced with permission from Ref. [46] Copyright 2017, Wiley-Blackwell. (b) Side and top views of Ti$_3$C$_2$T$_x$ (–OH termination) monolayer. (c) Side and top views of Ti$_3$C$_2$T$_x$ (-O termination) monolayer. (d) Additional lithium ions adsorbed on the -O terminations of the Ti$_3$C$_2$O$_2$Li$_2$ monolayers. Reproduced with permission from Ref. [51] Copyright 2014, American Chemical Society. SEM images of standard Ti$_3$C$_2$T$_x$ Mxene solution before and after exposure to air for 7 days (f), and for 30 days (g). Reproduced with permission from Ref. [58] Copyright 2017, American Chemical Society.

metastable behavior [59].

In view of the above findings, improving the oxidation resistance of MXenes and ensuring the preservation of their electrochemical and physical properties has been a research hotspot in recent years. Zhang et al. stored Mxene colloids in a sealed bottle filled with argon in a low-temperature environment, which considerably prolonged their storage life [58]. Chae et al. found that under a low enough storage temperature (-80 °C), the oxidation reaction of $Ti_3C_2T_x$ stagnates, prolonging its stability for more than 39 weeks [57].

The carbon/nitrogen atomic layer, namely the X layer, renders s MXene with excellent conductivity and increases the specific surface area of the material. The 2D carbon-based layered structure gives MXene the same remarkable properties as graphene. However, the most notable feature is the abundance of ion mosaic active sites per unit area that enable the reversible intercalation and deintercalation of Li^+, Na^+, K^+, Cs^+, Pb^{2+}, Mg^{2+}, Al^{3+}, and NH_4^+ plasmons. In addition to its incredible ability to accumulate energy, MXene has excellent mechanical and magnetic properties. Kurtoglu et al. [45] reported that MXene has a high modulus of elasticity when stretched along the base surface; specifically, its C_{11} value surpassed by almost 40% of the precursor MAX phase, but remained lower than that of graphene.

Guo et al. [60] studied the mechanical flexibility of Ti_2CT_x and found that its richness in hybrid terminations (e.g., -O) is key in enhancing its flexibility, allowing it to sustain increased strain. Undoubtedly, the robust mechanical properties of these materials offer vast application prospects in flexible capacitors. Furthermore, MXenes demonstrate unique electromagnetic properties. Because the valence electrons in the layered structure of transition metals are entirely free, and their valence states change with different bond formations, MXenes based on sundry bond states can exhibit diametrically opposite properties of ferromagnetism and anti-ferromagnetism. According to literature, Cr_2CT_x, Cr_2NT_x [59], and $Ta_3C_2T_x$ [62] are ferromagnetic, whereas $Ti_3C_2T_x$ and $Ti_3N_2T_x$ [63] behave exactly in the opposite manner. Xie et al. [64] discovered that the magnetism of MXene originates from 3D electrons of transition metal atoms, and functionalization of terminations outside the layer can be used as electron donors to combine with metal atoms, thus weakening or even eliminating the magnetism of the materials. The ferromagnetic properties of MXenes present broad application prospects for electromagnetic interference shielding and 2D spintronics [65].

3. Methods of synthesis

Currently, MXenes are produced by the selective etching of MAX; but early selective etching of MAX is an arduous process. Gogotsi, the pioneer of MXene, initially used various etching agents such as fluorine gas, hydrogen fluoride, and some molten salts (commonly used etchants for etching titanium and silicon); however, all these efforts were in vain. Although, they finally obtained a Ti-C-O-F cubic phase structure, it was not the ideal energy storage material [66]. Finally, a breakthrough was achieved by etching Ti_3AlC_2 in a hydrofluoric acid solution. They found that the Al layer in Ti_3AlC_2 could be dissolved by hydrofluoric acid, leaving a layered two-dimensional material of Ti_3C_2, which was the first MXene synthesis [10]. Thus, the technology to prepare MXenes has steadily advanced.

3.1. Solution etching methods

The solution etching of MAX phase, a selective exfoliation method to form MXene, is one of the most conventional and prevalent preparation methods. The core idea of this method is to utilize the strength difference between metal–metal and metal–carbon/nitrogen bonds to destroy the former while retaining the latter to achieve selective etching. The available etchants are divided into three main categories: (1) acid solutions, such as hydrofluoric acid (HF) [65,66], (2) mixed solutions of fluoride (LiF, NH_4F) and benign acids (HCl, H_2SO_4) [67,68], fluorine-containing acidic solutions (NH_4HF_2, NH_4F) [71,72], and (3) alkaline

solutions, such as potassium hydroxide (KOH, NH_4OH) [73] and successive use of acidic and alkaline solutions [74,75]. The first MXene, $Ti_3C_2T_x$ (Tx represents termination), was synthesized in this manner. Fig. 4a [10] shows the X-ray powder diffraction (XRD) patterns of Ti_3AlC_2 before and after selective solution-etching. The primary peak position of the material moved approximately from 401 to 101° (2θ), which demonstrates that the HF aqueous solution successfully etched the aluminum layer from the Ti_3AlC_2 phase. By comparing the main peak and remaining impurity peaks of the etched material, many similarities were found with the two (–OH) peaks of $Ti_3C_2F_2$ and Ti_3C_2, suggesting that $Ti_3C_2T_x$ (MXene) formed after the etching with HF aqueous solution contained both -F and –OH hetero-terminations. Raman spectroscopy (Fig. 4e [10]) showed that after etching the vibrational breakage of Al-Ti metal bonds induced the disappearance of peaks I, II, and III. Simultaneously, introducing hybrid terminations caused peaks IV, V, and VI to merge, broaden, and move down. The Raman pattern of this changing trend was consistent with the Raman features of very thin inorganic layered compounds [76,77]. In addition, it is worth noting that peaks V and VI were related to the oscillation of the Ti-C bond, which indicated that Al-Ti bond was destroyed by the etchant in contrast to Ti-C bonds. Finally, the existence of Ti-C and Ti-O bonds was observed in the X-ray photoelectron spectroscopy (XPS) spectra, further proving that etchant solution effectively introduced a variety of functional groups on the MXene surface during the solution etching treatment.

In the initial steps of the MXene synthesis process, HF was selected as the etchant to facilitate the insertion and extraction of ions during the electrochemical reaction and create more and larger spaces [78]. However, other cases of acid etching are rarely reported because most acid etchants will etch layer X, while etching layer A failed to achieve the purpose of selective exfoliation. The inventor of MXene, Naguib, used various etchants to etch MAX precursor before synthesizing the first MXene, but none of them achieved the purpose of selective etching, and a cubic product of Ti-C-O-F was obtained [66]. Parallelly, the HF aqueous solution was only used to selectively etch the MAX phase with the Al layer (A = aluminum layer) because of the bonding strength between different M and A elements. To achieve the selective exfoliation of different MAX phases, it was necessary to modify the etching environment (choice of etchant, etching temperature, etching time, etc.) to achieve selective exfoliation of different MAX phases [79].

Systematic research on solution etching has been conducted made by Naguib et al. [24] who used an HF aqueous solution to selectively etch Ti_2AlC, Ta_4AlC_3, $(Ti_{0.5}, Nb_{0.5})_2AlC$, $(V_{0.5}, Cr_{0.5})_3AlC_2$, and Ti_3AlCN precursors and obtained the expected MXene materials, thus verifying the feasibility of employing HF to exfoliate the Al-containing layer in the MAX phase. To further investigate the mechanism of HF-selective etching, Srivastav et al. [80] simulated the HF etching process using first-principles calculations and developed a theoretical model (Fig. 4d [80]). They pointed out that HF in aqueous solution intercalated from the edges of the MAX phase, forcing the Al layer to exfoliate. Simultaneously, the Ti atoms on the surface were gradually functionalized. With the continuous influx of HF into the MAX phase, the constant generation of AlF_3 and H_2 caused the material layer spacing to expand gradually and form a 2D structure. Finally, an MXene material with similar Gibbs free energy was formed.

Alhabeb et al. [81] investigated the effect of different concentrations of HF on the etching time of Ti_3AlC_2 at room temperature (RT) and discovered that the higher the consistency of the solution, the less the etching time required (e.g., 5 wt% for 24 h, 10 wt% for 18 h, and 30 wt% for 5 h). Su et al. [82] highlighted that an appropriate high temperature and ball milling are more conducive toward improving the etching efficiency and capacitance capacity of MXenes. Nevertheless, the disadvantages of HF etching began to manifest with more in-depth research.

As is well-known, HF is hazardous and must be handled carefully, with many researchers expressing concerns about the potential safety hazards and environmental problems caused by HF etching.
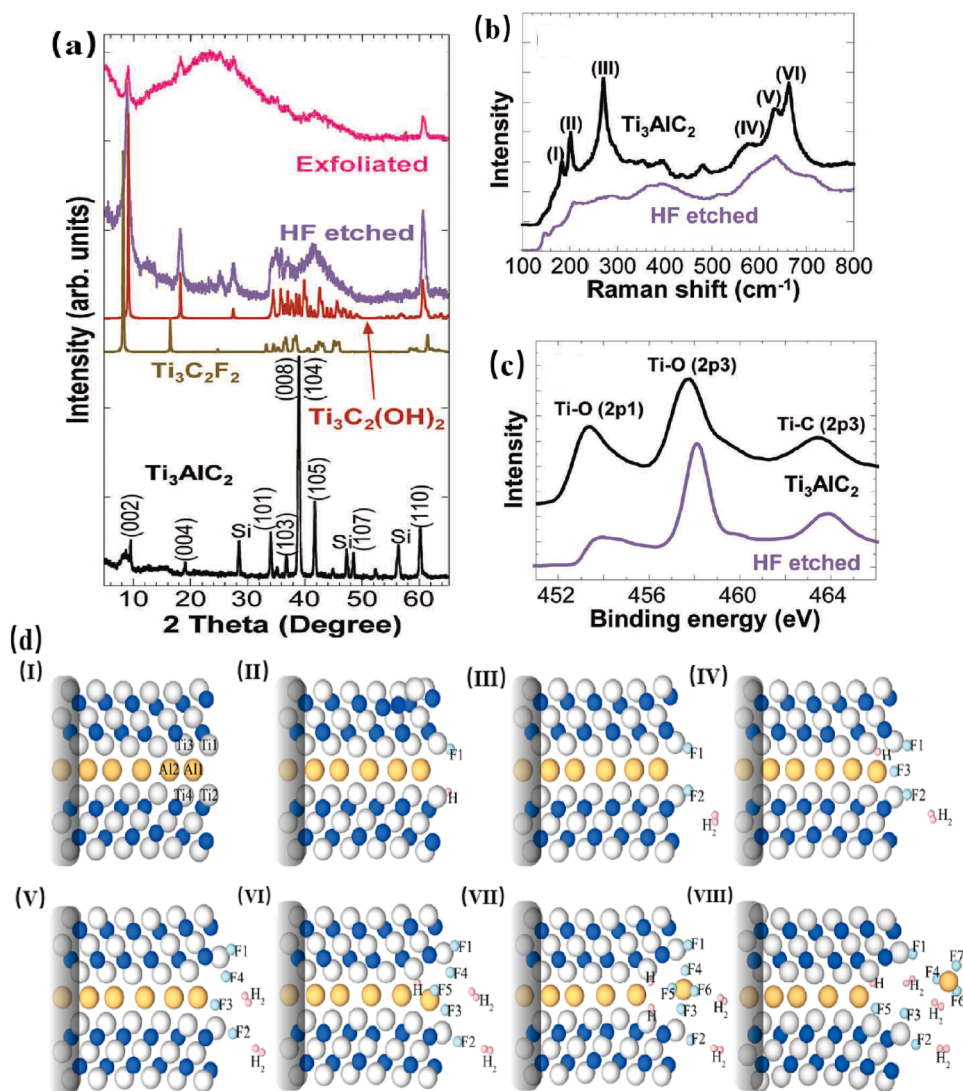
Fig. 4. (a) XRD patterns of Ti_3AlC_2 before and after etching and standard patterns of comparative materials. (b) Raman spectra of the material before and after etching. (c) XPS spectra of the material before and after etching. a, b, c) Reproduced with permission from Ref. [10] Copyright 2011, Wiley-Blackwell. (d) Mechanism of etching the lowest atomic energy configuration in an aqueous solution: (I) the original MAX phase (Ti_3AlC_2). (II-IV) The process of HF entering the MAX phase. (V-VII) The process of continuously generating H_2 and AlF_3. (VIII) The Al layer gradually peels off to form the MXene. The colors of silver, blue, orange, cyan, and pink represent Ti, C, Al, F, and H atoms, respectively. Reproduced with permission from Ref. [80] Copyright 2016, American Chemical Society. (For interpretation of the references to color in this figure legend, the reader is referred to the web version of this article.)

Additionally, the massive introduction of -F terminals during the HF etching process negatively impacts the adsorption and energy storage performances of MXenes [83,84]. Therefore, a series of novel solution etching methods have been developed. In 2014, a combination of fluoride salts (such as LiF, and KF) and more benign acids (such as HCl) was proposed for the selective etching of the MAX phase. Soundiraraju et al., [85] used KF salt and HCl to etch Ti_2AlN, successfully prepared Ti_2NT_x (MXene) and characterized the material. Liu et al. [86] combined HCl with LiF, NaF, KF, and NH_4F to etch Ti_3AlC_2 and Ti_2AlC to obtain MXene and found that cations in fluoride salt had a profound effect on the adsorption capacity of the material. Khazaei et al., [87] calculated the relationship between force constant and static exfoliation energy of the MAX phase and found that the total force constant of the A atom in the MAX phase was linearly related to the exfoliation energy, thereby predicting the minimum stripping energy required for the synthesis of MXene. This study provided valuable insights into new MXene preparation methods.

Zhang et al., [88] used a high-concentration KOH solution ($\approx$93.3 wt %) to etch Ti_3AlC_2 at 180 °C for 24 h and obtained unique MXene nanoribbons with abundant hydroxyl terminal groups, which showed excellent energy storage performance. Wu et al., [89] etched Ti_3AlC_2 using choline chloride and an oxalate-based deep eutectic solvent (DES) in the presence of NH_4F. Finally, MXene of 98% purity was successfully obtained, while the purity of the HF-etched MXene was 95%. Since the

first MXene synthesis in 2011, solution etching has been oriented towards green, mass production, and high-purity preparation. The synthesis of fluorine-free solutions has become a mainstream method for solution etching.

Solution etching is one of the most popular methods for synthesizing MXenes because of its high production efficiency, simple operation, and low cost. Wang et al., [90] etched Ti_3AlC_2 powder in an HF solution to obtain $Ti_3C_2T_x$ sheets. Then, a 3D interconnected 1-MoS_2/$Ti_3C_2T_x$ heterostructure was successfully prepared by combining MXene with 1 T-MoS_2 through hydrothermal and magnetic hydrothermal syntheses, and it was used in symmetric supercapacitors. The device exhibited a specific area capacitance of 347 mF/cm^2 at the scan rate of 2 mA/cm^2. Levitt et al., [91] placed a 3 g MAX phase with a mesh size of less than 45 um into 60 ml of a mixed solution containing 9 M HCl and 49% HF for selective etching. Finally, a multilayer $Ti_3C_2T_x$ was obtained, which was compounded with polyacrylonitrile (PAN) nanofibers to prepare a supercapacitor composite electrode material with good energy storage performance.

Li et al. [92] successfully synthesized $Ti_3C_2T_x$(X = –OH/-O) with high purity (92 wt%) using a completely HF-free alkali-assisted hydrothermal method. This green fluorine-free synthesis provides a new approach to the terminal group controllability of MXene. Zhang et al. [93] added 1 g Ti_3AlC_2 powder to a mixed solution containing 1 g LiF and 9 M HCl and subsequently stirred at 35 °C for 24 h to prepare a

$Ti_3C_2T_x$ MXene. Ghidiu et al. [94] mixed Ti_3AlC_2 with a solution of HCl and LiF. Finally, the clay-like filtrate was rolled after washing into a film to prepare $Ti_3C_2T_x$ clay. Remarkably, the supercapacitor electrode prepared from this clay showed an ultrahigh specific capacitance of 900F/cm^3 at a scanning rate of 2 mV/s, and almost no capacity loss after 10,000 cycles.

3.2. Electrochemical etching methods

Electrochemical etching is an environmental-friendly and efficient method for preparing MXenes with high energy consumption. The precursor MAX phase serves as an electrode that forms a circuit with a specific electrolyte to selectively remove the A layer under a particular voltage to obtain the MXene. The essence of the electrochemical etching process is the interaction between the electron flow and Gibbs free energy. If the established electrochemical reaction system is appropriate and the apparent voltage is correctly applied to the electrode materials, the expected selective shedding of the MAX phase can be realized [93,94]. Compared to solution etching, electrochemical selective etching utilizes the difference in the electron localization function (ELF) in the MAX phase to accomplish its goal. For example, in Ti_3AlC_2 materials, the ELF of Ti-C bonds is powerful (0.8–0.9), while that of Ti-Al bonds is relatively weak (0.4–0.6). Therefore, when the circuit is loaded with an appropriate voltage, the impact of electrons preferentially destroys the Ti-Al bonds and leads to the Al layer falling off to achieve selective etching [97].

Yin et al. [98] used a non-aqueous ionic [BMIM][PF6]-based solution as an electrolyte to establish an electrochemical etching system that could control the degree of surface fluorination, to prepare an MXene. Sun et al. [99] prepared an MXene by using dilute hydrochloric acid as the electrolyte and Ti_2AlC as the corrosion electrode. Although the MXene prepared by this method only contained -Cl, -O, and –OH groups, a certain amount of carbide-derived carbon (CDC) was detected in the MXene material owing to over-etching. Lukatskaya et al. [100] observed the etching of the MAX phase electrode into the CDC material when the electrochemical etching system was loaded with an excessive voltage. If the applied voltage window is too wide, it causes the M−A bond to break. After the A layer is completely peeled off, the M layer is further removed under the action of voltage, leaving only the amorphous carbon material. Therefore, in the electrochemical selective etching process, regulating the etching voltage is crucial. Pang et al. [101] fabricated ultrathin flower-like MXene flakes via electrochemical etching; however, the generation of the CDC layer impaired the etching efficiency of MXene during the preparation process. Therefore, it is necessary to develop a large-scale and high-efficiency MXene synthesis method that inhibits the growth of CDCs.

Despite the numerous advantages of electrochemical etching, such as being environmental-friendly and discarding the abuse of fluoride ions, concerns remain regarding the existence of CDCs [94,100]. In a recent study, Heidarpour et al., [103] prepared and characterized CDCs, highlighting their content in graphene, amorphous carbon, and other carbon structures. This implies that CDCs in specific structures may improve the energy storage performance of materials, suggesting that balancing the performance impact of CDCs and MXenes during electrochemical etching is a fascinating topic.

The advantage of electrochemical etching lies in its environmental protection and low energy needs, which are especially important given the world's unprecedented increase in energy consumption. In addition, electrochemical etching is entirely independent of the etchant, thereby avoiding the adverse effects of etchants on MXenes (introduction of fluorine-containing groups, low purity caused by the etchant, etc.) [104]. Cao et al. [105] electrochemically etched Ti_3AlC_2 in a low-risk NH_4HF_2 solution at room temperature, successfully obtaining $Ti_3C_2T_x$ in only 1.5 h at a voltage of 7.5 V. Zhao et al. [106] successfully prepared Cl- and N-doped $Ti_3C_2T_x$ MQDs (MXene quantum dots) via an electrochemical approach using Ti_3AlC_2 as the working electrode, Pt wire as the

counter electrode, and a mixed solution of 0.1 M tetramethylammonium hydroxide (TMAOH) and 0.2 M NH_4Cl as the electrolyte. The etching process was conducted at a low voltage of 0.1 V for 1 h, offering a new strategy for the green synthesis of MQDs. Mai et al. [107] synthesized a $Ti_3C_2T_x$/Cu composite structure via an electrochemical deposition approach for the first time, pointing out that the green and efficient electrochemical synthesis of MXene-based composite coatings has vital application prospects in tribology.

3.3. Molten salt methods

Molten salt synthesis is a green, environmental-friendly, highly efficient, and easy to operate method for the preparation of MXenes [108]. Its most striking feature is that it can effectively realize the control of MXene surface terminations, thus enabling a facile preparation of fluorine-free MXenes [109]. The preparation process is divided into four distinct steps. First, the reactants and salt compounds are mixed in an appropriate ratio; second, the salt in the mixture is heated in a specific atmosphere (vacuum, inert, reaction, or catalytic gas) to form a melt, thus creating a melting environment for the liquid phase; third, the reactants undergo a series of responses in a molten salt environment to develop new products with specific morphological characteristics; and finally, pure MXenes are obtained by washing. (Fig. 5a [110]). However, not every salt compound can be used to prepare MXenes using this method. Generally, salt is composed of ionic bonds and has a fixed melting temperature (T_m) and boiling temperature (T_b). When the temperature is higher than T_m, the salt is in a molten state, which provides a liquid reaction environment. In this fluid environment, the molten salt is endowed with higher diffusivity, further accelerating the chemical reactivity with the precursor phase [111].

To ensure the stability of the melt liquid-phase environment, it is necessary to choose a salt with an extreme temperature difference between T_m and T_b. Some salts of covalent compounds, such as $AlCl_3$, $FeCl_3$, and $ZnCl_2$, have continuous T_m and T_b values, implying that they are vaporized during melting, which destabilizes the liquid-phase reaction environment; therefore, they cannot be used as molten salts [112]. In addition, it should be noted that the grain size of the molten salt is a crucial factor in determining the product's success. Shi et al. [113] successfully refined commercial NaCl with a larger grain size (greater than100 μm) into a molten salt with a smaller grain size (10–30 μm) via a recrystallization process (Fig. 5c and d) [113]. In contrast to the smaller grain template, no 2D products were observed on the salt template with larger grain sizes.

The application of molten salt synthesissynthesis has led to the rapid development of nitrogen-based MXenes (transition metal nitrides (TMNs)). Until 2015, only carbon-based MXenes (transition metal carbons, TMCs) were prepared using HF and other etching techniques, while the breakthrough of TMDs stemmed only from first-principles calculations [61,102]. The preparation of TMN using conventional methods is challenging. One of the important reasons is that TMNs have higher forming energy than their precursor MAX phase, so it is difficult to peel off layer A from the nitrogen-based MAX phase selectively. However, TMNs are unstable in many etching solutions, so solvents easily dissolve them [100,110]. In the molten salt method, the etchant in the molten state mainly exists in the form of "naked" ions. These bare ions are not solvated, which significantly alleviates the high activation potential energy in the solvent deionization process. Therefore, bare ions in the molten salt system were more aggressive than their in-solution counterparts (Fig. 5e [114]).

Relevant research has shown that the reaction process of a perfect molten salt preparation system takes only a few minutes, achieving, on average a super-high preparation efficiency [116]. In addition, it is interesting that some materials are insoluble in water or other solvents but have high solubility in molten salts. Therefore, substances that solution synthesis approaches cannot prepare can often be prepared using the molten salt method [117]. Urbankowski et al. [118] mixed three
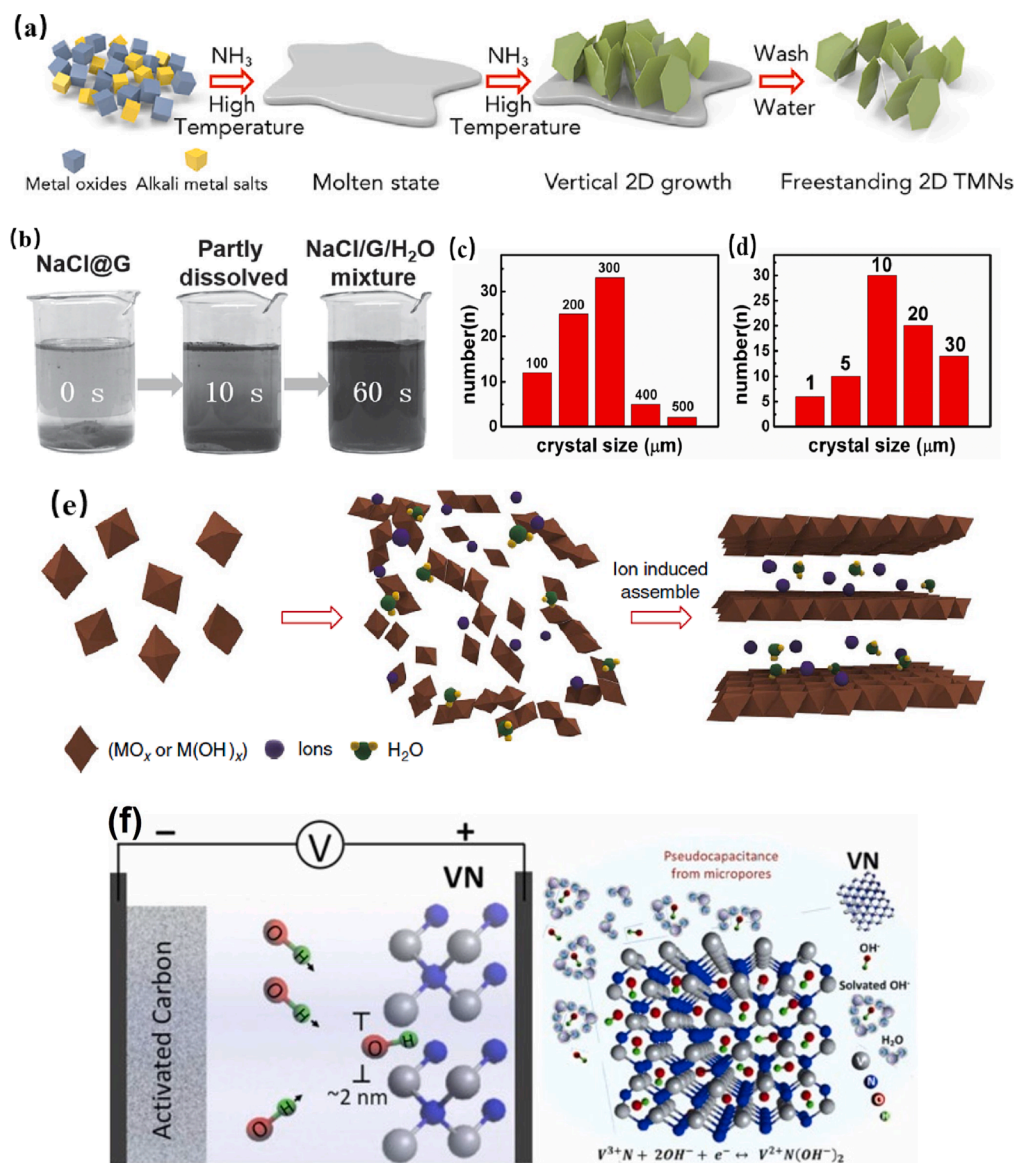
Fig. 5. (a) Molten salt synthesis process. Reproduced with permission from Ref. [110] Copyright 2020, Elsevier. (b) Recrystallization process after molten salt solution. (c) Crystal size and distribution of commercial NaCl salts. (d) Crystal size and distribution of recrystallized NaCl powder. Reproduced with permission from Ref. [113] Copyright 2015, Wiley-VCH. (e) Etching mechanism of agent-naked ions and accelerated 2D structure formation during molten salt synthesis. Reproduced with permission from Ref. [114] Copyright 2017, Springer Nature. (f) Pseudocapacitive reaction mechanism of 2D TMN electrodes, taking VN as an example. Reproduced with permission from Ref. [115] Copyright 2019, Elsevier.

fluoride salts (KF, NaF, LiF) with MAX for the first time and prepared $Ti_4N_3T_X$ under an argon atmosphere at 550 °C, creating a precedent for experimental research on TMN materials. The prepared MXene contained fluoride salt impurities that needed to be further purified. Arole et al. [119] mingled Ti_3AlC_2 with SnF_2, heated it in an argon atmosphere for 6 h to prepare $Ti_3C_2T_x$, and successfully prepared water-dispersible MXene by KOH washing. Guo et al. [120] mixed $Ti_3C_2T_X$ (MXene with -F terminations) with $LiCl$-KCl-K_2CO_3 co-molten salt, followed by heating at 450 °C for 12 h. The results showed that the -F terminals were mostly replaced by -O terminals during molten salt synthesis. Furthermore, the intercalation of K^+ ions also increased the interlayer spacing of the 2D structure, thus greatly improving the energy storage performance.

Additionally, 2D TMN exhibits strong pseudo-capacitance due to its nitrogen-rich phase [121], which brings the energy storage effect of MXene to a new level. As shown in Fig. 5f [115], the surface of TMN electrode can undergo rapid redox reaction with the OH– ions, and such a fast and reversible Faradaic reaction makes the TMNs possess excellent energy storage properties (more details, shown in section 4). Overall, the molten salt method offers significant scope for the development of high-efficiency synthesis of MXenes, especially the 2D TMN.
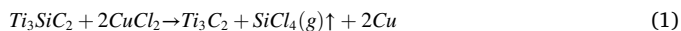
3.4. Lewis acidic etching methods

In recent years, the Lewis acidic etching method has become the most popular synthesis method for MXenes. This synthesis method is similar to the molten salt approach discussed above; however, its etching mechanism is entirely different. Considering that this method has significantly promoted the MXene material family in the emerging supercapacitor material field, it is necessary to distinguish it from molten-salt synthesis.

Lewis acid etching method is also known as the element replacement approach [122]. Lewis acid salts produce metal cations with strong electron acceptors in the molten state, which can efficiently react with the metal elements in the MAX phase to selectively discard the A layer [118,119]. Compared to conventional molten salts, Lewis acid salts are generally transitioned metal halides, such as $CuCl_2$, $ZnCl_2$, CuI, $ZnBr_2$. This series of covalent compounds cannot be used in the traditional molten salt method because of their continuous T_m and T_b values [112]. When MAX phase of the precursor is immersed in a Lewis molten salt, the metal cation dissociated from the Lewis molten salt undergoes a displacement reaction with the metal in the A layer, resulting in a gas-phase halide salt. With the volatilization of the gas-phase halide salt, the A layer is selectively etched, thus forming a 2D structure. Finally,

pure MXene is obtained by washing the product. (Fig. 6a [124]). It is worth noting that a two-step chemical reaction equation can describe the whole preparation process. Taking the reaction of Ti_3SiC_2 (precursor) and $CuCl_2$ (Lewis acid salt) as an example, this synthesis involves the following reactions [124]:

$$Ti_3SiC_2 + 2CuCl_2 \rightarrow Ti_3C_2 + SiCl_4(g)\uparrow + 2Cu \qquad (1)$$

$$Ti_3C_2 + CuCl_2 \rightarrow Ti_3C_2Cl_2 + Cu \qquad (2)$$

The essence of the reaction is to provide the redox potential of the molten salt and precursor phase and then realize the selective etching of the MAX phase by the Gibbs free energy replacement reaction. Li et al. [124] demonstrated that an ideal MXene could be successfully prepared when the Lewis salt satisfies the Gibbs free energy substitution reaction conditions in a high-temperature melting state. They constructed a mapping of the Gibbs free energy reaction and proposed a general strategy for synthesizing MXene using a Lewis molten salt (Fig. 6b [124]).

The preparation method is not only green, safe, and entirely fluorine-free, but also has the significant advantage of extending and bridging various extra-layer functional groups (T_x). Generally, almost all MXene terminals are dominated by -O,–H, and –OH groups [125]. In 2020, Kamysbayev et al. [126] synthesized various MXenes, such as $Ti_3C_2Br_2$, TI_2CBr_2, and Ti_2CCl_2, by Lewis molten salt etching. Compared with traditional MXenes (with -F and –OH groups), MXenes with -Cl and -Br terminal groups are covalently functionalized easily. Then, the -Br and -Cl groups are substituted by chemical reactions to form -O, –NH, -S, -Se, and -Te terminal groups, which not only achieves the covalent modification of MXenes, but also expands their performance development potential (Fig. 6i [126]). Undoubtedly, covalently functionalized terminals push the MXene material family to a new research era; however, reports on the properties and synthesis methods of covalently functionalized MXenes are still lacking.

Lewis acid etching is an emerging strategy for the preparation of MXenes. This method is environment-friendly, safe, controllable, and, most notably, it can introduce covalent functional terminal groups in MXenes [126]. Perhaps the most promising attribute of this strategy is its potential for modifying the T_x of MXenes. Luo et al. [127] reported a simple one-step Lewis acid-etching method for the synthesis of MXenes. They reacted Ti_3AlC_2 with Lewis acid $CoCl_2$ at 750 °C to prepare a Co-modified MXene composite. The prepared MXene had a -Cl terminal and exhibited enhanced electrochemical performance [99]. In addition, the intercalation of Co further increased the interlayer spacing of the MXene, thus improving its energy storage effect.

Zeng et al. [128] synthesized a Prussian blue analogues@MXene and investigated the degradation performance of coumarin. The results showed that the Lewis acid site of the MXene was critical for the degradation performance. Khan et al. [129] prepared $Ti_3C_2Cl_2$, $Ti_3C_2I_2$, and $Ti_3C_2Br_2$ by mixing Ti_3AlC_2 with $CuCl_2$, CuI_2, and $CuBr_2$ Lewis acid salts, respectively. They studied the pseudo-capacitance behavior of the materials, which showed fast charge and discharge rates in a 3 M H_2SO_4 electrolyte, with specific capacitances of 92, 29, and 63C/g, respectively. In addition, many studies have shown that the surface of MXene has abundant Ti sites that promote the interaction between Lewis acids and polysulfides and increases the chemical adsorption capacity of polysulfides [130–132]. This result is vital for lithium-sulfur batteries and MXene-based polysulfide composite pseudocapacitors.

3.5. Other synthesis methods

Numerous emerging preparation methods have been reported along with the in-depth study of MXene materials. MXenes prepared using these methods exhibit different shapes and properties. Although the synthetic methods discussed here are not mainstream, they still deserve attention. For example, MXene thin films with ultrahigh charge conductivities that are suitable for electronic parts and electrode materials

have been prepared via vacuum filtration (Fig. 7a [133]) and rolling (Fig. 7b [134]). In addition, spin coating (Fig. 7c [135]) and painting (Fig. 7d [136]) techniques have also been used to prepare MXene films with micron-scale thickness, which are suitable for optical and electronic components. Further, spray coating (Fig. 7e [137]) has been widely used in the preparation of large-area films for electromagnetic shielding owing to its efficient forming method.

Huang et al. [138] reported vacuum-filtration-assisted synthesis strategy for designing MXene/carbon nanotube@MnO$_2$ composite pseudocapacitor electrode. The prepared capacitor device demonstrated energy and power densities of 24.5 mW·h/cm^3 and 2.5 W/cm^3, respectively. Tian et al. [139] successfully prepared a silicon/MXene composite paper by following a vacuum filtration synthesis method, and utilized it in a lithium-ion battery. They discovered that this synthesis method effectively alleviated the re-stacking of MXene sheets, while providing them with additional active sites, promoting ion transport, and improving their energy storage performance. Yang et al. [140] synthesized an MXene-boron nitride-MXene flexible supercapacitor by rolling. They discovered that the mesopores and macropores of the MXene layer were densified during rolling, increasing its density and making the structure more rigid.

Qin et al. [141] prepared an MXene-based translucent electrode via spin coating and used it in a supercapacitor. This research profoundly impacts the flexible design of MXenes and their application in photovoltaic energy. Li et al. [142] injected ultrathin $Ti_3C_2T_x$ nanosheets into the electrode materials of supercapacitors using spraying technology to form an MXene/NiCo$_2$S$_4$@carbon fiber cloth flexible electrode. They found that the injected MXene nanosheets effectively improved the conductivity of the electrode, which demonstrated an ultrahigh specific capacity of 2326F/g at a current density of 1 A/g. Finally, chemical vapor deposition (CVD) [143], physical vapor deposition (PVD) [144], and atomic layer deposition (ALD) [145] have also been used in the synthesis of MXene thin films. These methods effectively reduced the oxidation and hybridization ends of MXene.

Appropriate preparation of MXene with an ideal structure using different synthesis methods is the key to improve the properties of the materials. The formation of a unique MXene design heavily relies on the initial preparation environment. Therefore, exploring the mapping relationship between the synthesis method and final product structure is still an important research topic.

4. Applications in pseudosupercapacitors

4.1. Charge storage mechanism

The main energy storage mechanisms of EDLC capacitors are divided into the reversible electrosorption of ions on the surface of the material and fast reversible redox reactions that occur near the surface and interior of the material. This paper mainly discusses pseudocapacitance. The prefix pseudo comes from the Greek word pseûdos, which means approaching, almost, or trying to be. Unlike EDLCs, pseudocapacitive energy storage originates from the Faraday effect. It involves the back-and-forth movement of charges between two layers of electrodes that causes a potential difference during the charge movement, similar to battery charging and discharging. Since this energy storage mechanism is similar to that of a battery, but not identical, it is called pseudocapacitance [146].

Owing to their fast electron transport capabilities, MXenes have greatly contributed to the energy storage performance of pseudocapacitors. During MXene-assisted pseudocapacitive energy storage in an aqueous solution, various ions reversibly intercalate the MXene layers and occupy the electrochemically active sites on the MXene surface, thus realizing the energy storage mechanism [147,148]. In this type of pseudocapacitance energy storage, the reversible insertion and removal of charged ions cause the c-lattice parameters to fluctuate. The fluctuation value decreases with an increase in voltage (Fig. 8a [149]),
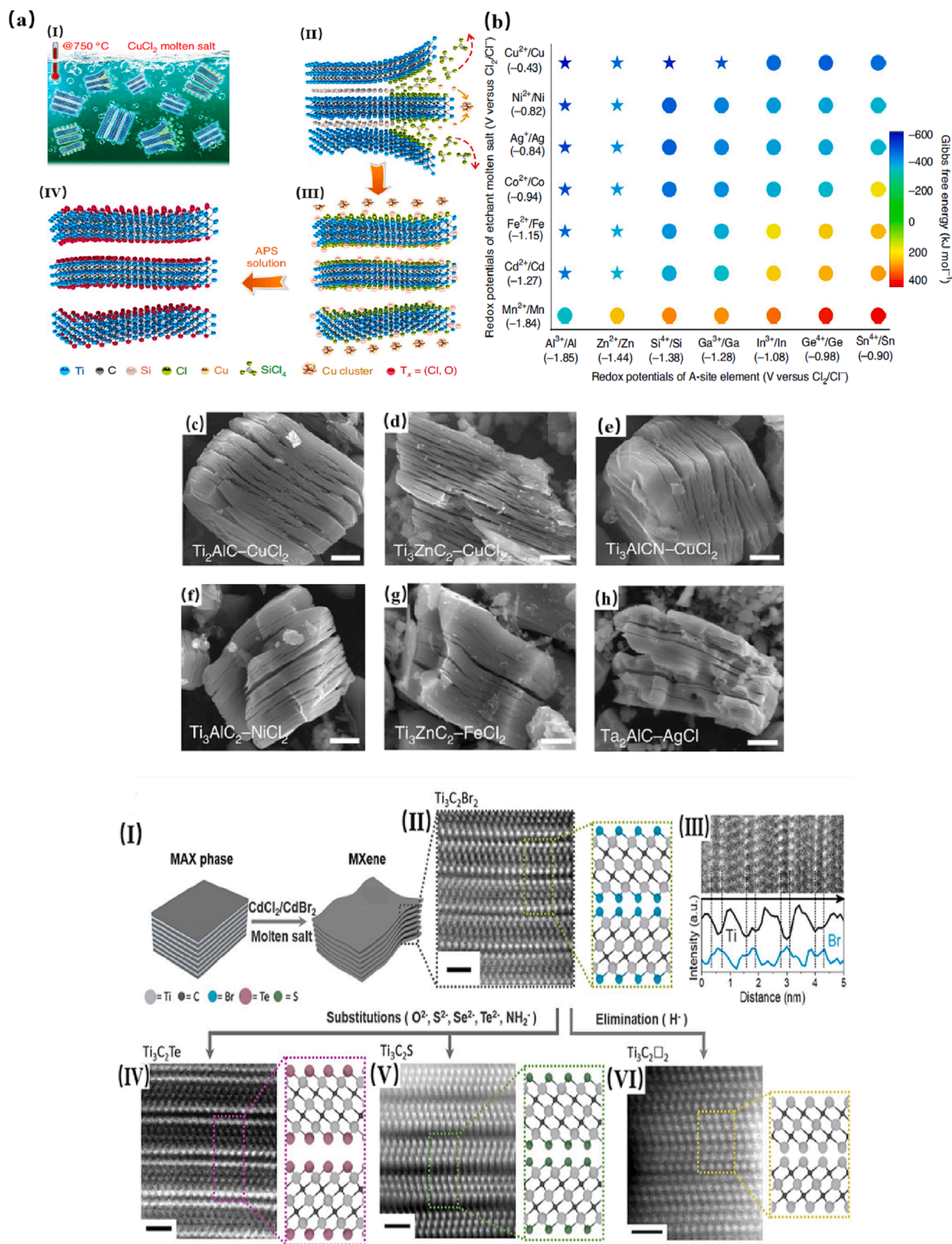
Fig. 6. (a) Schematic of Lewis Acidic Etching Methods. (I) MAX precursor is immersed in Lewis molten salt. (II) Metal cations react with elements in layer A by substitution. (III) Gas-phase halide salt evaporates and separates to form a 2D structure. (VI) MXene is obtained after further washing. (b) Gibbs free energy diagram (700 °C) is used to guide the selection of Lewis acid Cl salts: the A layer element of the MAX precursor (X-axis), the cation of the Lewis acid Cl salt (Y-axis), and the star shape have been demonstrated experimentally, and the dot shape is the theory. (c-h) Etching of different MAX phases obtained by MXene micromorphology with diverse Lewis Cl salts. (c) Ti_2AlC by $CuCl_2$. (d) Ti_3ZnC_2 by $CuCl_2$. (e) Ti_3AlCN by $CuCl_2$. (f) Ti_3AlC_2 by $NiCl_2$. (g) Ti_3ZnC_2 by $FeCl_2$. (h) Ta_2AlC by AgCl. Reproduced with permission from Ref. [124]. Copyright 2020, Springer Nature. (i) Covalent functionalization process of MXene surface: (I) Lewis acid salt etching process. (II) The atomic resolution high-angle annular dark-field (HAADF) image of $Ti_3C_2Br_2$ MXene. (III) Energy dispersive X-ray (EDX) analysis of $Ti_3C_2Br_2$ MXene. (IV) The HAADF image of Ti_3C_2Te. (V) The HAADF image of Ti_3C_2S. (VI) The HAADF image of $Ti_3C_2\square_2$ ($\square$ Represents vacancy). Reproduced with permission from Ref. [126]. Copyright 2020, American Association for the Advancement of Science.
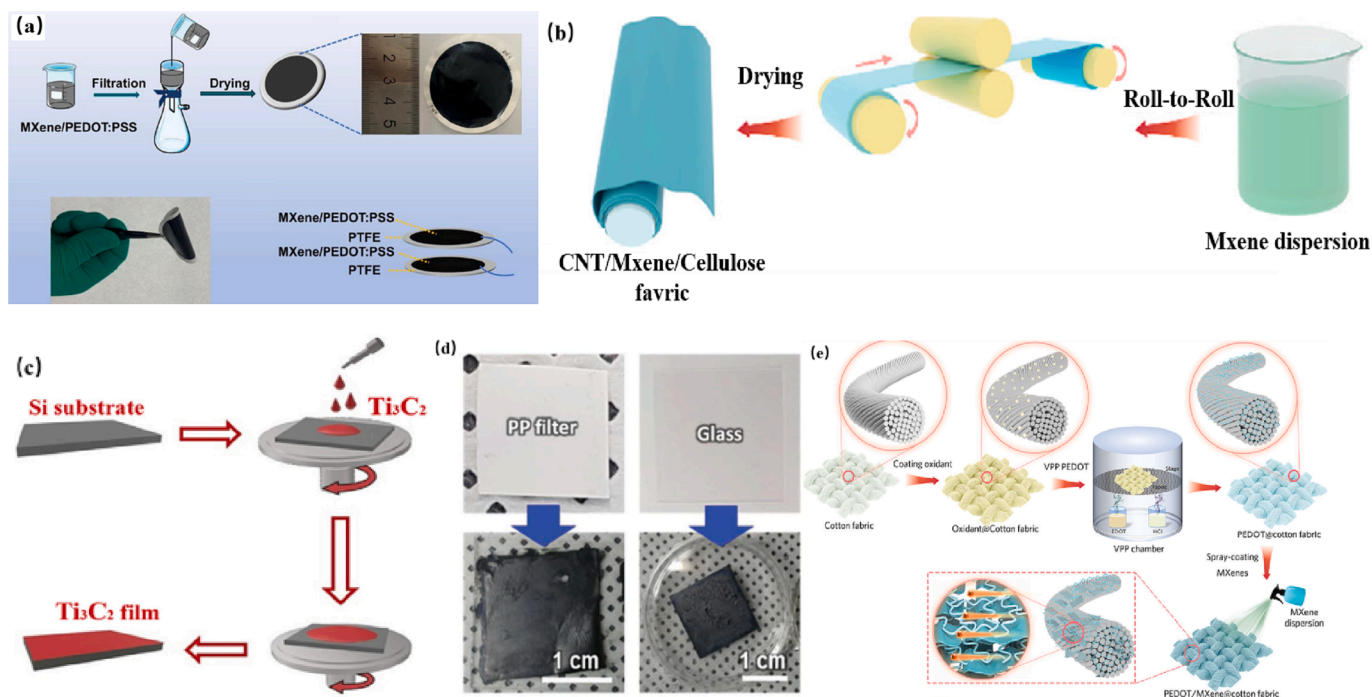
Fig. 7. (a) Illustration of MXene synthesis by filtration. Reproduced with permission from Ref. [133] Copyright 2021, Elsevier. (b) Illustration of MXene synthesis by rolling. Reproduced with permission from Ref. [134] Copyright 2021, Elsevier. (c) Illustration of MXene synthesis by spin coating. Reproduced with permission from Ref. [135] Copyright 2019, Elsevier. (d) MXene thin films prepared on different substrates using brushes. Reproduced with permission from Ref. [136] Copyright 2021, Royal society of chemistry. (e) Uniform MXene film prepared on fiber fabric by spraying. Reproduced with permission from Ref. [137] Copyright 2021, Royal society of chemistry.

confirming that the pseudocapacitance of MXene is mainly due to the number of active sites embedded by reversible ions on the surface of the material. Therefore, the layered structure of MXene provides suitable adsorption sites for these active sites, which are called deep and shallow adsorption sites (Fig. 8b [150]). In addition, pseudocapacitors exhibit characteristic cyclic voltammograms (CV) and galvanostatic charge–discharge curves (GCD). Fig. 8c-k shows the CV for different types of capacitors, whereas Fig. 8e, 8 h, and 8 k demonstrate the GCD curves. Pseudocapacitor materials usually conform to one or several combinations of Figs. b, d, and e [147].

4.2. Advantages of MXene-based pseudocapacitors

As a new energy storage material with high volume-specific capacity and energy density, MXene has attracted much attention. In particular, the abundant functional groups outside the layer are considered active sites that can effectively promote and activate the insertion and removal of active ions between layers and interfaces/surfaces [151]. In addition, the unique morphology of MXene contributes to the electrochemical performance of the pseudocapacitors to a certain extent. For instance, following the etching of layer A from the MAX phase, 2D slits are formed that can trap some water molecules inside and thus enhance the material's capacitance [24,152]. Furthermore, owing to the negative dielectric constant of water, the dipole polarization of these water molecules can shield the external electric field and further augment capacity. In addition, the smaller lateral dimension of the layer allows it to boost ion diffusion and enhance capacitance more than other conventional materials [153].

Many studies have demonstrated the tailorable morphology of 2D MXene materials, suggesting that MXene-based pseudocapacitors are marginally affected by factors, such as shape, size, processing difficulty, or extrusion deformation. This dramatically expands the application prospects of MXenes in the energy field. Huang et al. [154] reported symmetrical MXene-based micro-supercapacitors (MSCs) (Fig. 9a),

whose ultrasmall volume, high working voltage, and high power density offer broad prospects in the field of high-precision integrated circuits. HU et al. [155] prepared a $Ti_3C_2T_x$ solid-state supercapacitor and tested its capacitance performance under various bending, twisting, and knotting conditions. The deformation state maintained good capacitance performance, which was attributed to the unique flexible structure of the materials. Wang et al. [156] processed an MXene material into a flexible film and then designed a new super flexible capacitor endowed with a 3D ion transport channel with excellent mechanical properties. Guo et al. [157] reported an all-solid-state (ASS) ultrathin MXene-based supercapacitor with small volume and high energy density and applied it to an energy emergency system. In view of the above examples, it can be inferred that the energy storage advantages of MXenes (compared to other materials) in the field of supercapacitors are not only limited to their remarkable energy storage performance but also their adaptiveness and adjustability under changeable and complex load environments (Fig. 10).

4.3. Mxene-based pseudocapacitors

As one knows, the most significant advantage of the supercapacitor is its long cycle life, high power density, and no need for manual maintenance, which is the foundation of the green sustainable project. However, its low energy density has always been criticized; therefore, batteries and supercapacitors are always a dilemma. The formula for calculating the energy density of supercapacitors is as follows [158]:

$$E = \frac{C \times V^2}{2 \times 3.6} \tag{3}$$

where C is the specific capacitance, and V is the operating voltage window. Therefore, there are two methods to improve the energy density of MXene-based pseudocapacitors: expanding the voltage window and increasing the specific capacitance.
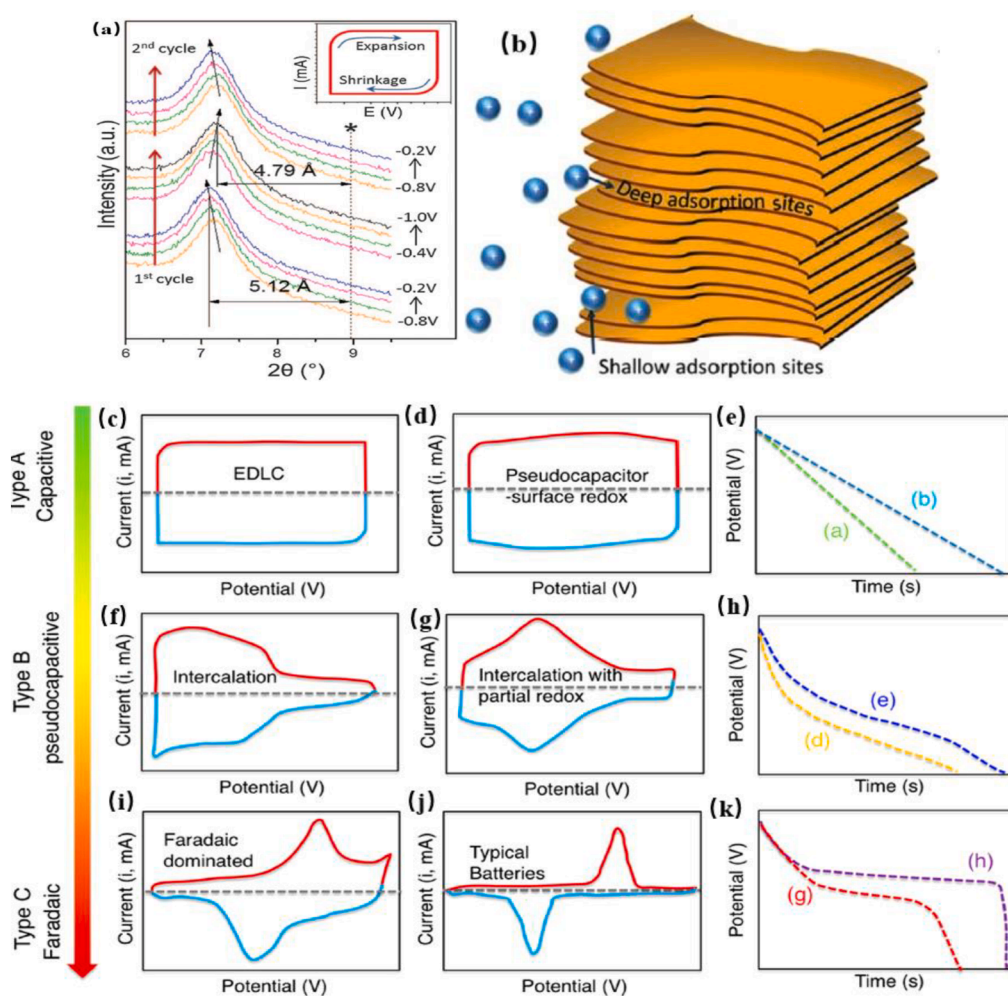
Fig. 8. (a) In-situ XRD analysis showing the lattice parameter changes caused by ion insertion and removal at different potentials ($Ti_3C_2T_x$ in 1 M KOH solution). Reproduced with permission from Ref. [149] Copyright 2013, American Association for the Advancement of Science. (b) Active site provided by the specific layered structure of MXene. Reproduced with permission from Ref. [150] Copyright 2015, Wiley-VCH. (c, d, f, g, i, j) CV schematic diagrams: (c) EDLC materials; (d) surface redox materials; (f) intercalation materials; (g) intercalation with partial redox materials; (i) Faradaic-dominated materials; (j) typical battery materials. (e, h, k) Galvanostatic discharge curves. Reproduced with permission from Ref. [147] Copyright 2018, American Chemical Society.

4.3.1. Extended pseudocapacitor working voltage window

The working voltage window of the capacitor is related to the electrode material, electrolyte, and current collector. Therefore, when the electrode materials of the MXene-based pseudocapacitor are determined, it is possible to increase the working voltage window by using an appropriate current collector, organic solution/ionic liquid, or by assembling an asymmetric pseudocapacitor. Generally, platinum, nickel foam, and carbon paper as capacitor current collectors are used to lower the decomposition voltage of the solvent. Lukatskaya et al. [159] used glassy carbon as the current collector to test the electrochemical performance of MXene and found that the voltage window could be extended to 1 V in 3 M H_2SO_4. In addition, graphite and Ti foils can expand the voltage window. On the other hand, the appropriate ionic electrolyte can also effectively improve the working voltage of MXene.

Lin et al. [160] used an EMI-TFSI ion electrolyte with $Ti_3C_2T_x$ gel to successfully control the working voltage to 0–3 V with a capacitance of 70F/g at a scanning speed of 20 mV/s. In situ XRD results showed that the capacitance and working voltage window behavior of MXene may be changed by the polarization of the ionic liquid or the change in ion intercalation [161]. Finally, it has been hot research in recent years has focused on increasing the working voltage via the design of an asymmetric pseudocapacitor to enhance the energy density. Related investigations include MXene// carbon-based materials (graphene, CNT, rGO, etc.), MXene// metal oxides (V_2O_5, RuO_2, etc.), MXene// polymers (polyaniline, etc.), and other systems. Li et al. [162] assembled wavy-layered $Ti_3C_2T_x$ MXenes with carbon-based materials (rGO/CNT/PANI ternary composites) to form a fully asymmetric pseudocapacitor. Its working voltage window increased significantly, showing a high volume

energy density of 70 Wh/L, and its stable working voltage was about 1.45 V. Wei et al. [163] mixed MXene with carbon fiber to form an MXene//MnO_2 asymmetric all pseudocapacitor, and its working voltage window reached 1.5 V. The voltage was more than twice that of the symmetrical device and had a high energy density of 6.4 Wh/kg. However, owing to the compatibility of asymmetric capacitor materials, the difference between the actual and theoretical specific capacities of the positive and negative electrodes and the range of the electrolyte voltage window, there are still few reports on the mechanism of MXene-based asymmetric pseudocapacitors.

4.3.2. Improving pseudo-capacitance of MXene

The pseudocapacitance of MXene only involves a rapid and reversible redox reaction on the surface and near the surface of the material. Therefore, it is only related to the number and density of active sites on the surface of the material and its conductivity but has nothing to do with the specific surface area and pore size distribution (which needs to be distinguished from the EDLC capacitance here). The following are some common ways to improve the pseudocapacitance of MXenes.

4.3.2.1. Intercalation and dispersion modification. Intercalation and dispersion modification effectively use an intercalation agent to embed the MXene layered structure to expand the interlayer spacing and prevent material stacking and aggregation. It is only necessary to mix the MXene and intercalating agent sufficiently during intercalation for ultrasonic vibration dispersion [164]. Many intercalation agents are available, including dimethyl sulfoxide (DMSO), TBAOH, and TMAOH
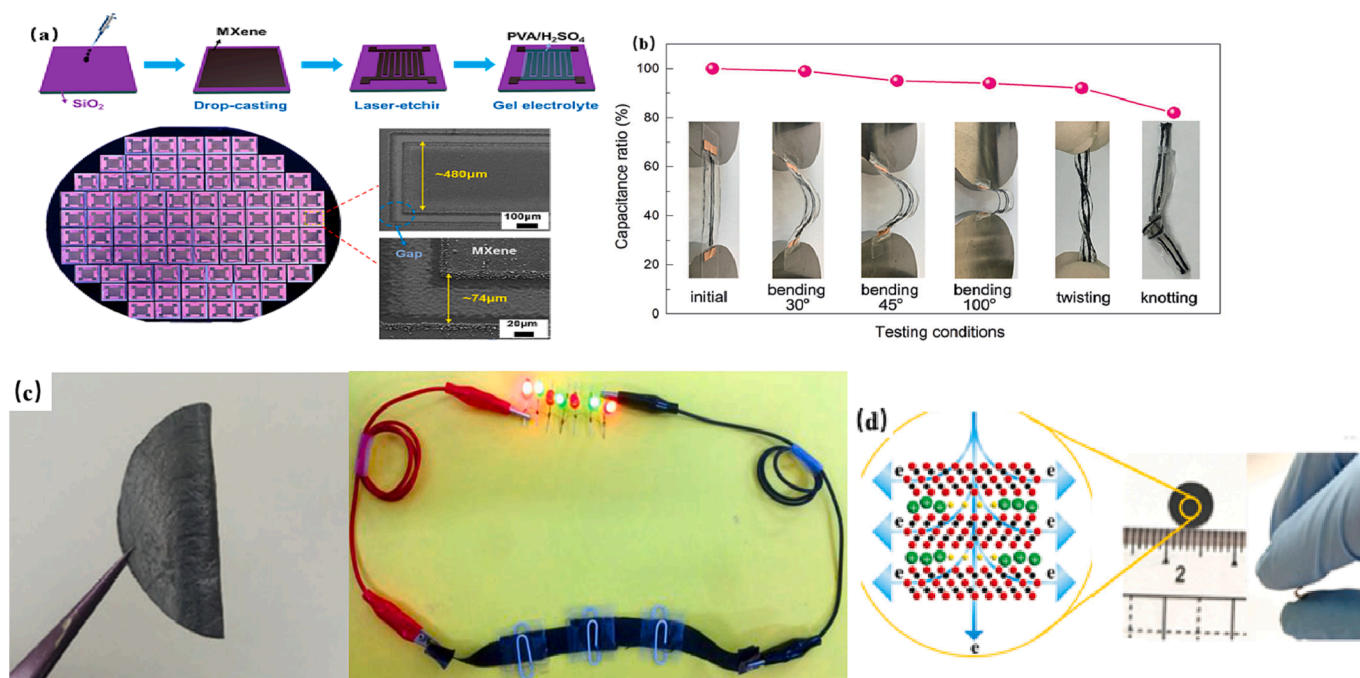
Fig. 9. (a) MXene-based ($Ti_3C_2T_x$) on-chip micro-supercapacitors. Reproduced with permission from Ref. [154] Copyright 2022, ACS Publications. (b) Normalized capacitance (C/C_0, where C_0 is the initialization capacitance) of all-fiber MXene-based ($Ti_3C_2T_x$) supercapacitors in various deformation modes (scan rate 20 mv/s). Reproduced with permission from Ref. [155] Copyright 2017, Wiley-VCH. (c) MXene flexible film and MXene-based supercapacitor power supply system. Reproduced with permission from Ref. [156] Copyright 2019, Wiley-VCH. (d) Ultra-thin ASSS MXene supercapacitor electrodes. Reproduced with permission from Ref. [157] Copyright 2019, Wiley-VCH.

[165]. The pseudocapacitance enhancement of MXene by intercalation and dispersion modification is mainly due to two factors. First, the interlayer spacing of MXene is increased to expose more active sites, thus increasing the number of redox reactions. The other is that the distribution and types of groups on the surface of MXene change during intercalation, which will significantly change the energy storage performance of MXene according to first principles [51]. Boota et al. [166] systematically compared the effects of nonpolar, polar, and alkyl chain polymer intercalation on the pseudocapacitance of MXene. The results showed that polar intercalation of the alkyl chain increased the interlayer spacing more easily, thus improving the specific capacity and cycle stability.

Tomar et al. [167] prepared a $Ti_3C_2T_x$-based perovskite-oxide composite electrode and intercalated it with cations and anions. Layered MXene and perovskite oxide showed cationic and anionic intercalation pseudo-capacitances, respectively. This study revealed a new double-ion intercalation field and provided a new idea for new MXene intercalation. Yang et al. [168] used ammonium citrate (AC) as an all-in-one intercalant, antioxidant, and nitrogen source and then annealed MXene in ammonia. It was found that the doping efficiency of the pre-intercalated MXene was higher, and the pseudocapacitor performance was better.

4.3.2.2. Doping. Although MXene research has made extraordinary progress in energy production, common MXene-based energy materials are unsatisfactory. Studies have shown that doping strategies can effectively improve the functional surface structure of MXene and its energy storage performance [169]. Doped elements can not only generate or promote the generation of pseudo-capacitance but also improve its wettability in electrolytes and promote the diffusion of electrolyte ions. For the non-mental co-doping, N, P, and S doping strategies have been widely proven to be practical and feasible for significantly improving the electrochemical performance of MXene [170–172]. Liu et al. [173] successfully synthesized 4.5 at.% N-doped Nb_2CT_x MXene using urea as a nitrogen source in hydrothermal synthesis. It was found that the lattice parameter of N-doped MXene

increased from 22.32 Å to 34.78 Å, showing a higher specific capacitance. For the metal co-doping, polyvalent metal particles can increase the pseudo-capacitance reaction of MXene. Gao et al. [174] prepared V-doped $Ti_3C_2T_x$ MXene nanosheets via hydrothermal synthesis. Because V^{3+} and V^{4+} ions form V-C and V-O species on the surface of MXene, the V-doped MXene exhibits extremely high pseudo-capacitance, with the highest capacitance of 365.9F/g at 2 M KCl(10 mV/s scanning speed). In addition, element doping can change the energy band structure of the MXene material transforming its behavior from semiconducting to conducting [175].

Yang et al. [176] reported a solvothermal treatment with nitrogen doping. The solution used was a urea-saturated alcohol solution or monoethanolamine, which provided a nitrogen source for $Ti_3C_2T_x$. Compared with in situ solid N doping, MXene doped with a non-in situ N solvent showed a higher capacitance. Notably, the pair of electrons and π-conjugated rings was found in the XPS spectra, which significantly reduced their resistance. At present, improving the doping methods, such as developing in situ doping and exploring the doping of diversified elements and composite elements, are the most important for improving the electrochemical performance of MXene and realizing its theoretical capacity.

4.3.2.3. Mxene-based composites. A single MXene material has the same defects as all 2D materials. It is easy to stack and collapse between layers, which reduces its effective specific surface area and buries its active sites, resulting in a waste of capacity [12,153]. The formation of a composite structure with other excellent electrode materials can effectively adjust the overall frame performance of MXenes to improve their electrochemical performance. To date, tremendous efforts have been made to explore emerging MXene-based composites for Pseudosupercapacitors owing to their remarkable synergistic effect and broad application prospects.

A compound with a semiconductor material forms a heterojunction composite material. MXene has a small band gap, and its band gap lies between that of the conductor and semiconductor [59,172]. Therefore,
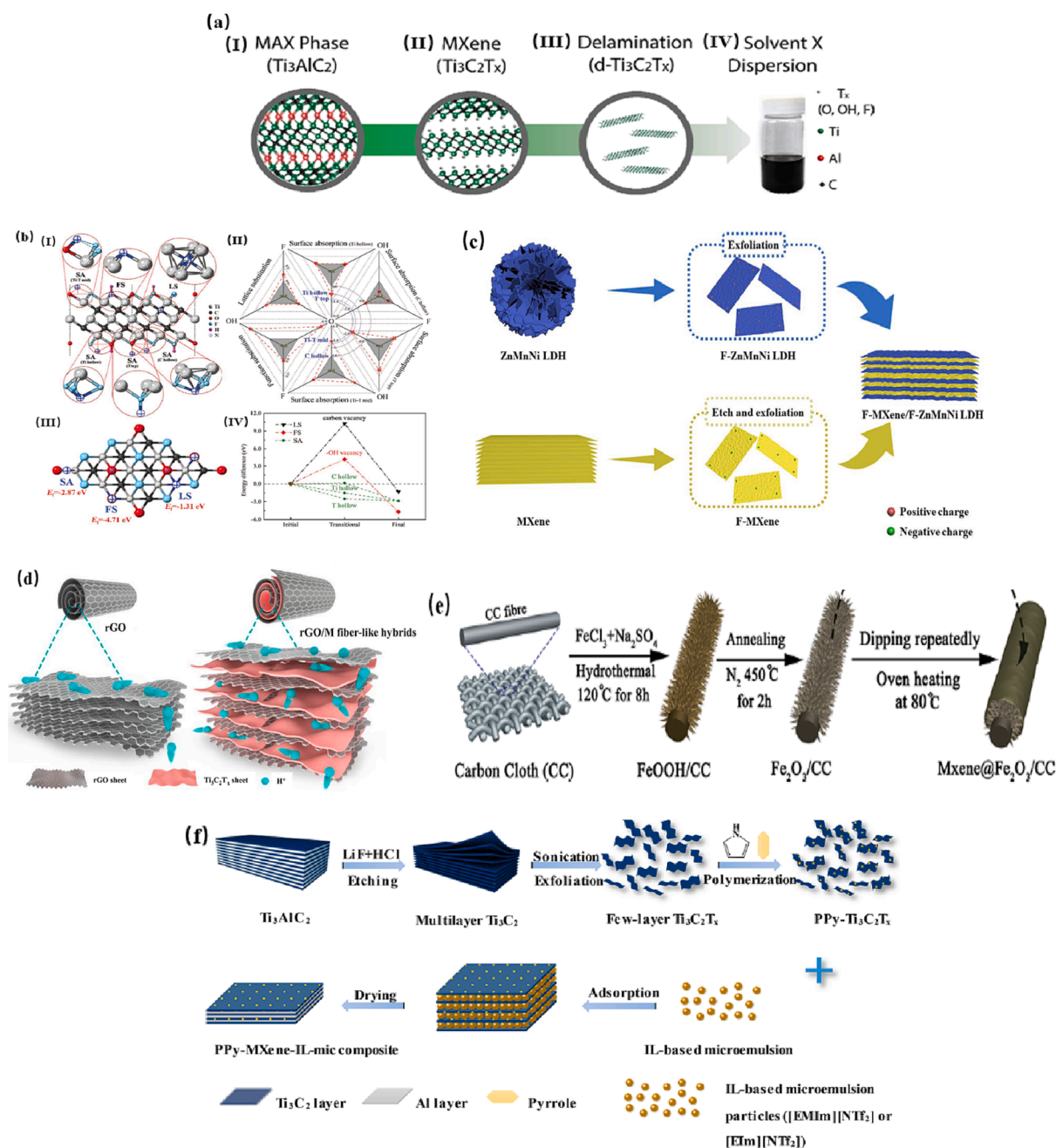
Fig. 10. Various methods of improving MXene pseudo-capacitance. (a) Schematic of intercalation and dispersion modification of MXene. (I) The original MAX phase (Ti$_3$AlC$_2$). (II-III) The preparation process of MXene. (III-IV) Process of intercalation and dispersion via sonication or intercalating agent. Reproduced with permission from Ref. [164] Copyright 2017, American Chemical Society. (b) Schematic of MXene nitrogen doping (Take Ti$_3$C$_2$T$_x$ as an example). (I) Atomic structure diagram of nitrogen-doped MXene, including all doping sites. (II) Forming energy calculation results (the shaded part is positive). (III) Schematic of the doped unit cell (top view). (IV) The calculation result of the transition energy state. Reproduced with permission from Ref. [170] Copyright 2020, Wiley-VCH. (c) Schematic of the formation of self-assembled van der Waals heterostructure MXene matrix composites. Reproduced with permission from Ref. [179] Copyright 2020, American Chemical Society. (d) Composite of MXene and carbon-based materials (rGO). Reproduced with permission from Ref. [181] Copyright 2020, Elsevier. (e) Schematic of composite synthesis of MXene (T$_3$C$_2$T$_x$) and transition metal oxide (Fe$_2$O$_3$). Reproduced with permission from Ref. [186] Copyright 2019, Royal Society of Chemistry. (f) Schematic of the composite formation mechanism of MXene and a conductive polymer. Reproduced with permission from Ref. [33] Copyright 2022, Elsevier.

MXene can be combined with other semiconductor materials to form MXene-based heterostructured electrode materials. Jiang et al. [178] prepared a 2D layered Co(OH)$_2$/TiC$_2$T$_x$ heterojunction electrode. The TiC2Tx loading was 25 wt%, and its total pseudo-capacitance was twice that of bare Co(OH)$_2$. The pseudocapacitance can reach 153.0F/g, and the capacitance only decreased by 1% after 1000 cycles. Sun et al. [179] compounded MXene with layered double hydroxides (LDHs) to form Ti$_3$C$_2$T$_x$/ZnMnNi LDH van der Waals heterostructured electrodes. The

heterostructure combines the outstanding electronic conductivity and stability of MXene, high theoretical specific capacity, and rich redox active sites of LDHs. It showed an ultra-high pseudo-capacitance of 2,065F/g at a scanning rate of 5 mV/s, and a capacitance retention rate of 99.8% after 100,000 cycles at a current density of 1 A/g. Lin et al. [180] used Ti$_3$C$_2$T$_x$ MXene as a multifunctional interface modifier between the InGaN nanorods and Si for the first time. They formed type-II band alignment in the InGaN/MXene heterojunction and an Ohmic

junction at the MXene/Si interface, which significantly reduced the resistance of the semiconductor and electrolyte heterojunction and obtained an 82% fast hole injection efficiency and excellent stability.

Compounding with carbon-based materials can increase the effective SSA and prevent local collapse and stacking of material edges. Although a large SAA does not contribute to the pseudo-capacitance, it reduces the wrinkles of the material, leading to exposure to more active sites, especially the deep adsorption sites that are often buried in the cracks of the lamellae. Generally, the carbon materials to be compounded are carbon nanotubes, graphene, and their derivatives. Wang et al. [181] compounded fibrous redox graphene with MXene, and the results showed that the rGO/MXene hybrid had more micropores and exposed more active sites, thus increasing the capacitance. In addition, the rGO sheet effectively inhibited the oxidation of MXene and improved the cycle performance. The volumetric capacitance was approximately $345.2F/cm^3$, and the gravimetric value was approximately 195F/g at 0.1 A/g.

HU et al. [182] reported the binding effects of redox-active molecules on $Ti_3C_2T_X$ and CNT. These active molecules were beneficial for expanding the working voltage window, thus improving the overall capacitance and energy density. Yang et al. [183] compounded $Ti_3C_2T_x$ MXene with porous g-C_3N_4 nanosheets to form composite Schottky junctions. The results showed that the formation of Schottky between MXene and g-C_3N_4 and the built-in electric field at the interface accelerated the charge separation in the internal space of the material, inhibited the recombination of electron-hole pairs, and thus improved the efficiency of photogenerated electrons. Zhang et al. [184] prepared three-dimensional $Ti_3C_2T_x$ MXene/ rGO/ carbon (MGC-500) flexible hybrid electrode using a template method. This composite electrode material has high pseudocapacitance and good energy storage performance under various deformation conditions.

Compounding with transition metal oxides and derivatives can obtain higher pseudocapacitance owing to the polyvalent metal in the electrode/solution interface reaction process. Zheng et al. [185] bridged $Ti_3C_2T_x$ MXene and MoO_3 nanobelts with different mass ratios. The results showed that when the mass ratio was 8 (MoO_3):2 ($Ti_3C_2T_x$), the composite material exhibited the best performance, showing pseudo-capacitance of 837C/g and $1836C/cm^3$ at a current of 1 A/g. This was because the randomly oriented MoO_3 nanobelts prevented MXene nanoplate stacking, thus exposing more active sites. Li et al. [186] coupled $Ti_3C_2T_x$ MXene with Fe_2O_3 nanorod arrays immersed in carbon cloth (CC) to form a composite anode and used MnO_2/CC as the cathode. It was found that multivalent Fe ions in Fe_2O_3 can provide the composite with higher electrochemical activity and large specific capacitance, while the MXene layer provided not only capacitance for flexible electrodes, but also fast and efficient ion/electron transmission path for the Fe_2O_3, thus effectively improving the electronic conductivity, power density, and energy density of the capacitor.

A metal–organic framework (MOF) was introduced to fabricate MX-based composites with better electrochemical performance and flexibility. MOFs are structures composed of metal clusters or ions that form coordination bonds with organic ligands. These unique frameworks provide materials with high surface areas and adjustable pore sizes [187]. Xie et al. [188] developed $CoFe_2O_4$ nanorods from MOFs and combined them with MXene nanosheets. They observed that cobalt iron oxide can act as a support frame between MXene layers, increasing the spacing between 2D structural layers and preventing material stacking. In addition, Co-Fe also provides active sites for energy storage, which promotes charge transfer, and a volume capacitance of $2467.6C/cm^3$ is obtained in the LiCl electrolyte. From the pseudo-capacitance energy storage mechanism, introducing transition metal elements with multivalent state changes to form a composite structure with MXene is the most direct and effective method to improve pseudo-capacitance.

Compounding with a conductive polymer can make the composite material produce higher Faraday pseudo-capacitance in the process of charge and discharge; hence, it is also a standard method to improve the

performance of MXene-based pseudo-capacitance [189]. Fan et al. [33] inserted polypyrrole (PPy) particles and ionic liquid (ILs)-based micro-emulsion particles as double spacers into the interlayer structure of $Ti_3C_2T_x$ MXenes. It was found that these polymer particles can effectively avoid the stacking collapse of MXene layers and, at the same time, contribute to the ideal capacitance of hybrid materials and increase the cyclic stability of the materials themselves. Ling et al. [190] composited $Ti_3C_2T_x$ with poly-diallyl dimethylammonium chloride (PDDA) or electrically neutral polyvinyl alcohol (PVA) to synthesize $Ti_3C_2T_x$/ polymer composites. The synthesized composite films exhibited excellent electrochemical performances. The specific capacity of the composite film electrode with a thickness of only 13 um prepared by filtration with a microporous membrane was $528F/cm^3$ in 1 mol/L KOH electrolyte at a scanning speed of 2 mV/s. Muhammad et al. [166] compounded $Ti_3C_2T_x$ with polyfluorene derivatives and studied its electrochemical properties. They pointed out that charged polar polymers containing nitrogen are polymers with the strongest binding tendency toward MXene. They can significantly increase the interlayer spacing, thus making it possible to insert more organic materials into the MXene layers.

MXene and its modification methods to improve the performance of pseudocapacitor electrodes are listed in Table 1. MXene and its composites show excellent performance in the field of supercapacitors; however, MXene is still in the development stage, and much research and exploration are needed regarding its mechanism and modification technology.

5. Opportunities and future challenges

Significant efforts have been made to design and develop new pseudocapacitor electrode materials based on MXenes, and remarkable results have been achieved. The preparation and modification of MXenes are the two crucial technical strategies for improving the energy storage performance of materials. In the synthesis of MXenes structures with more active sites, larger energy storage spaces, and lower resistivities specifically favor pseudocapacitance. Specifically, controlling the carbon/nitrogen layer (X layer), transition metal layer (M layer), and extra-layer terminations (T_x) of MXene by adjusting the etching method, etchant concentration, etching time, and precursor phase, are critical steps for adjusting and controlling the rapid and reversible redox reactions of the materials. For example, the transition metal layer (M) exhibits higher pseudocapacitance characteristics because of its multivalent metals.

The nitrogen/carbon layer (X) can often improve the cycle reversibility of the entire material and ensure structural stability because of its large specific surface area and strength. However, different functional groups in the extra-layer terminal (T_x) are not unique. For instance, it is well known that the F terminal is not conducive to inserting and removing electrons and ions. On the other hand, material modification, such as intercalation, dispersion, recombination, heterojunction formation, and doping, can also compensate for the inherent shortcomings of 2D materials and enhance their energy-storage performance. In recent years, research on the modification of MXenes has increased exponentially, proving the feasibility of these methods.

The problems faced by the MXenes still need to be resolved. First, the development of emerging selective etching technology is the top priority. At present, most of the MXenes are still in the early stages of theoretical synthesis, and there is no effective way to selectively etch their precursor MAX [11], which dramatically limits the expansion of MXene family members. In addition, most etching methods will produce external terminations that are not conducive to energy storage performance [217]. Therefore, it is necessary to further modify the surface of MXene. Secondly, despite their prolonged existence in the industry, their commercialization is still to be achieved. At present, there are few reports on the commercial preparation of MXenes in large quantities. The cost of experimental preparation is too high, and the preservation

Table 1

Different strategies used for improving the pseudocapacitance of MXenes.

Materials	Modification method	Device type	Specific capacitance	Current density/ sweep rate	Cycling retention	Ref.
$Ti_3C_2T_x$	Intercalation	Supercapacitor electrode	517F/g	1 A/g	10 000/99%	[191]
$Ti_3C_2T_x$	Intercalation	Supercapacitor electrode	380F/g	2 mV/s	10 000/98%	[166]
F-free $Ti_3C_2T_x$	Intercalation	All-solid-state flexible supercapacitor	439F/cm^3	10 m/s	10 000/~90%	[97]
$Ti_3C_2T_x$	Intercalation	All-solid-state flexible supercapacitor	256F/cm^3	5 m/s	10 000/ 92.4%	[192]
N, O co-doped C @$Ti_3C_2T_x$	Doping	Symmetric supercapacitor	250.6F/g	1 A/g	5000/94%	[193]
N-doped $V_4C_3T_x$	Doping	Supercapacitor electrode	210F/g	10 mV/s	10 000/96.3%	[194]
N-doped $Ti_3C_2T_x$	Doping	Supercapacitor electrode	156F/g	5 mV/s	5000/100%	[195]
N-doped $Ti_3C_2T_x$	Doping	Supercapacitor electrode	192F/g	1 mV/s	10 000/92%	[196]
N, S co-doped $Ti_3C_2T_x$	Doping	Supercapacitor electrode	175F/g	5 mV/s	5000/90.1%	[197]
N-doped d-$Ti_3C_2T_x$	Doping and dispersion	Supercapacitor electrode	266.5F/g	5 mV/s	2000/86.4%	[198]
V-doped $Ti_3C_2T_x$	Doping	Supercapacitor electrode	365.9F/g	10 mV/s	5000/95%	[174]
$Ti_3C_2T_x$/ Ni-Co-Al-LDH	Heterojunction	All-solid-state flexible supercapacitor	748.2F/g	1 A/g	10 000/97.8%	[13]
$Ti_3C_2T_x$ /CoAl-LDH	Heterojunction	Symmetric supercapacitor	2472C/cm^3	1 A/g	30 000/94.4%	[199]
$V_4C_3T_x$/NiCoAl-LDH	Heterojunction	Hybrid supercapacitors	627C/g	1 A/g	10 000/98%	[200]
d-$Ti_3C_2T_x$/Ni$_3$S$_2$	Heterojunction and dispersion	Hybrid supercapacitors	2204F/g	1 A/g	5000/76.3%	[201]
$Ti_3C_2T_x$/MoS$_2$	Heterojunction	Micro-supercapacitors	383F/g	1 mV/s	6000/98%	[202]
$Ti_3C_2T_x$/MoS$_2$	Heterojunction	Supercapacitor electrode	303.8F/g	1 A/g	10 000/72.3%	[203]
$Ti_3C_2T_x$/rGO	Composite with carbon-based materials	All-solid-state flexible supercapacitors	405.5F/g	1 A/g	10 000/100%	[204]
$Ti_3C_2T_x$/rHGO	Composite with carbon-based materials	Symmetric supercapacitors	1445F/cm^3	2 mV/s	10 000/93%	[205]
$Ti_3C_2T_x$/BCN	Composite with carbon-based materials	All-solid-state supercapacitors	1173F/g	2 A/g	100 000/ 100%	[206]
RuO$_2$@$Ti_3C_2T_x$	Composite with transition metal oxide	Micro-supercapacitors	864.2F/cm^3	1 mV/s	10 000/90%	[207]
$Ti_3C_2T_x$/ Ni-MOF	Composite with MOF	Supercapacitor electrode	1124F/g	1 A/g	4000/74.8%	[208]
$Ti_3C_2T_x$/Co(OH)$_2$	Composite with transition metal derivatives	Supercapacitor electrode	153F/g	0.5 A/g	1000/99%	[178]
MnO$_2$@$Ti_3C_2T_x$	Composite with transition metal oxide	Flexible and symmetric supercapacitors	390F/g	10 mV/s	6000/93%	[209]
$Ti_3C_2T_x$/Bi$_2$S$_3$	Composite with transition metal derivatives	Symmetric supercapacitors	615C/g	3 A/g	1000/91%	[210]
$Ti_3C_2T_x$/ppy	Composite with conductive polymer	Pseudocapacitive electrodes	416F/g	5 mV/s	25 000/92%	[211]
$Ti_3C_2T_x$/BC@Ppy	Composite with conductive polymer	Micro-supercapacitors	388 mF/cm^2	1 mA/cm^2	25 000/95.8%	[212]
$Ti_3C_2T_x$/PDDA	Composite with conductive polymer	Supercapacitor electrode	528F/cm^3	2 mV/s	10 000/~99%	[190]
$Ti_3C_2T_x$/ppy	Composite with conductive polymer	All-solid-state supercapacitors	406F/cm^3	100 mV/s	20 000/ ~100%	[213]
CNT/Ti$_2$CT$_x$	Composite with conductive polymer and intercalation	Supercapacitor electrode	515.3F/g	2 mV/s	5 000/95.3%	[214]
NiCo$_2$-LDHs@$Ti_3C_2T_x$/ rGO	Composite with carbon-based materials	Hybrid supercapacitor	240F/g	1 A/g	10 000/92.8%	[215]
Ni$_x$Al$_y$(OH)$_2$/$Ti_3C_2T_x$	Composite with transition metal hydroxides	Supercapacitor electrode	1061F/g	1 A/g	4000/70%	[216]

conditions are too harsh (unable to be preserved for a long time). Investigating the stability of MXene is crucial in advancing the commercialization of energy storage devices based on MXene. Thirdly, although considerable research focus has been devoted to the performance characterization of MXenes after the synthesis and modification stages, their energy storage mechanism is still to be completely explored. The research on energy storage mechanism of 2D materials has reached a level of depth (atomic layer level) that cannot be explained through conventional means. There is still a significant gap existing in the current understanding of the mechanisms involved in energy storage research. Some researchers have recently started the study of the mechanism of MXenes by in situ characterization or molecular dynamics simulations [218], bringing a new research direction to the study of energy storage materials at the atomic level. However, the biggest flaw of MXenes lies in stacking and collapsing their material edges, which reduces SSA and burying the active points. This is also the root cause of their limited theoretical capacity. At present, alleviating stacking and collapsing phenomena in 2D materials is the core challenge.

6. Conclusions

This review discusses the historical development of novel 2D MXene material family, including the main synthesis strategies, unique properties, and specific applications in the field of pseudocapacitive supercapacitors. The energy storage challenges that have become increasingly urgent in the past decades have led to the innovation of supercapacitors. This review provides a comprehensive report on MXene-based capacitors to facilitate the exploration and discovery of advanced energy storage systems by integrating the latest research results with regard to their structural properties, pseudocapacitive energy storage mechanisms, and modification methods.

MXene is a 2D layered material with advantageous features, including hydrophilicity, high conductivity, and adjustable functional terminal groups. Reports have constantly emerged in the past few decades, specifically on $Ti_3C_2T_x$ MXenes. In addition, pseudocapacitors have higher power and energy density than ordinary supercapacitors (because of the occurrence of redox reactions on their surfaces), thus providing a possible route to tackle the current energy dilemma. The research and development of MXenes in the field of pseudocapacitance are met with the trends: (1) preserving the composite structure design of MXenes and further improving their specific capacity and energy storage properties; (2) exploring the emerging flexible and miniature pseudocapacitors and expanding their application environment, particularly from the aspects of high load, high extrusion deformation, high precision, and delicate applications; (3) developing green, fluorine-free, and terminal-controlled MXene synthesis methods (especially in recent

years, covalent functional groups have been newly introduced, expanding the family of functionalized MXene materials [122] exponentially); (4) design and development of hybrid pseudocapacitors with widened working voltage windows and improved energy density features; (5) finally, MXenes also have the potential in ion kinetic batteries due to their ability to undergo fast and reversible redox reactions during the energy storage. Its 2D layered structure can be combined with different energy materials for more efficient energy storage. It is hoped that future studies will resolve these issues.

Declaration of Competing Interest

The authors declare that they have no known competing financial interests or personal relationships that could have appeared to influence the work reported in this paper.

Data availability

No data was used for the research described in the article.

Acknowledgments

References

[1] K. Swart, Trends in the energy market after World War II (WW II), J. Power Sources. 37 (1992) 3–12, https://doi.org/10.1016/0378-7753(92)80059-K.

[2] A. Kundu, N.P. Shetti, S. Basu, K.R. Reddy, M.N. Nadagouda, T.M. Aminabhavi, Identification and removal of micro-and nano-plastics: Efficient and cost-effective methods, Chem. Eng. J. 421 (2021), 129816, https://doi.org/10.1016/j.cej.2021.129816.

[3] A. Mishra, N.P. Shetti, S. Basu, K. Raghava Reddy, T.M. Aminabhavi, Carbon cloth-based hybrid materials as flexible electrochemical supercapacitors, ChemElectroChem 6 (2019) 5771–5786, https://doi.org/10.1002/celc.201901122.

[4] T. Tavangar, M. Karimi, M. Rezakazemi, K.R. Reddy, T.M. Aminabhavi, Textile waste, dyes/inorganic salts separation of cerium oxide-loaded loose nanofiltration polyethersulfone membranes, Chem. Eng. J. 385 (2020), 123787, https://doi.org/10.1016/j.cej.2019.123787.

[5] C.V. Reddy, I.N. Reddy, R. Koutavarapu, K.R. Reddy, T.A. Saleh, T. M. Aminabhavi, J. Shim, Novel edge-capped ZrO$_2$ nanoparticles onto V$_2$O$_5$ nanowires for efficient photosensitized reduction of chromium (Cr (VI)), photoelectrochemical solar water splitting, and electrochemical energy storage applications, Chem. Eng. J. 430 (2022), 132988, https://doi.org/10.1016/j.cej.2021.132988.

[6] J. Gopinath, R.K.C. Balasubramanyam, V. Santosh, S.K. Swami, D.K. Kumar, S. K. Gupta, V. Dutta, K.R. Reddy, V. Sadhu, A.V.S. Sainath, T.M. Aminabhavi, Novel anisotropic ordered polymeric materials based on metallopolymer precursors as dye sensitized solar cells, Chem. Eng. J. 358 (2019) 1166–1175, https://doi.org/10.1016/j.cej.2018.10.090.

[7] W. Zhang, G.E. Eperon, H.J. Snaith, Metal halide perovskites for energy applications, Nat. Energy. 1 (2016), https://doi.org/10.1038/nenergy.2016.48.

[8] M. Cakici, R.R. Kakarla, F. Alonso-Marroquin, Advanced electrochemical energy storage supercapacitors based on the flexible carbon fiber fabric-coated with uniform coral-like MnO$_2$ structured electrodes, Chem. Eng. J. 309 (2017) 151–158, https://doi.org/10.1016/j.cej.2016.10.012.

[9] C.V. Reddy, K.R. Reddy, R.R. Zairov, B. Cheolho, J. Shim, T.M. Aminabhavi, g-C$_3$N$_4$ nanosheets functionalized yttrium-doped ZrO$_2$ nanoparticles for efficient photocatalytic Cr (VI) reduction and energy storage applications, J. Environ. Manage. 315 (2022) 115120, https://doi.org/10.1016/j.jenvman.2022.115120.

[10] M. Naguib, M. Kurtoglu, V. Presser, J. Lu, J. Niu, M. Heon, L. Hultman, Y. Gogotsi, M.W. Barsoum, Two-dimensional nanocrystals produced by exfoliation of Ti$_3$AlC$_2$, Adv. Mater. 23 (2011) 4248–4253, https://doi.org/10.1002/adma.201102306.

[11] Y. Gogotsi, B. Anasori, The rise of MXenes, ACS Nano 13 (2019) 8491–8494, https://doi.org/10.1021/acsnano.9b06394.

[12] M. Hu, H. Zhang, T. Hu, B. Fan, X. Wang, Z. Li, Emerging 2D MXenes for supercapacitors: status, challenges and prospects, Chem. Soc. Rev. 49 (2020) 6666–6693, https://doi.org/10.1039/d0cs00175a.

[13] S. Sun, C. Liao, A.M. Hafez, H. Zhu, S. Wu, Two-dimensional MXenes for energy storage, Chem. Eng. J. 338 (2018) 27–45, https://doi.org/10.1016/j.cej.2017.12.155.

[14] Y. Sun, D. Chen, Z. Liang, Two-dimensional MXenes for energy storage and conversion applications, Mater. Today Energy 5 (2017) 22–36, https://doi.org/10.1016/j.mtener.2017.04.008.

[15] J.-C. Lei, X. Zhang, Z. Zhou, Recent advances in MXene: Preparation, properties, and applications, Front. Phys. 10 (2015) 276–286, https://doi.org/10.1007/s11467-015-0493-x.

[16] L. Hou, W. Yang, Y. Li, P. Wang, B. Jiang, C. Xu, C. Zhang, G. Huang, F. Yang, Y. Li, Dual-template endowing N, O co-doped hierarchically porous carbon from potassium citrate with high capacitance and rate capability for supercapacitors, Chem. Eng. J. 417 (2021), 129289, https://doi.org/10.1016/j.cej.2021.129289.

[17] N.R. Reddy, A.S. Kumar, P.M. Reddy, R.R. Kakarla, S.W. Joo, T.M. Aminabhavi, Novel rhombus Co$_3$O$_4$-nanocapsule CuO heterohybrids for efficient photocatalytic water splitting and electrochemical energy storage applications, J. Environ. Manage. 325 (2023), 116650, https://doi.org/10.1016/j.jenvman.2022.116650.

[18] K. Shireesha, T.R. Kumar, T. Rajani, C.S. Chakra, M.M. Kumari, V. Divya, K. Raghava Reddy, Novel NiMgOH-rGO-based nanostructured hybrids for electrochemical energy storage supercapacitor applications: effect of reducing agents, Crystals 11 (2021) 1144, https://doi.org/10.3390/cryst11091144.

[19] J. Yan, Q. Wang, T. Wei, Z. Fan, Recent advances in design and fabrication of electrochemical supercapacitors with high energy densities, Adv. Energy Mater. 4 (2014) 1300816, https://doi.org/10.1002/aenm.201300816.

[20] M. Naguib, V.N. Mochalin, M.W. Barsoum, Y. Gogotsi, 25th anniversary article: MXenes: a new family of two-dimensional materials, Adv. Mater. 26 (2014) 992–1005, https://doi.org/10.1002/adma.201304138.

[21] M.W. Barsoum, MAX phases: properties of machinable ternary carbides and nitrides, John Wiley & Sons, 2013.

[22] B. Anasori, Y. Xie, M. Beidaghi, J. Lu, B.C. Hosler, L. Hultman, P.R.C. Kent, Y. Gogotsi, M.W. Barsoum, Two-dimensional, ordered, double transition metals carbides (MXenes), ACS Nano 9 (2015) 9507–9516, https://doi.org/10.1021/acsnano.5b03591.

[23] B. Anasori, M.R. Lukatskaya, Y. Gogotsi, 2D metal carbides and nitrides (MXenes) for energy storage, Nat. Rev. Mater. 2 (2017), https://doi.org/10.1038/natrevmats.2016.98.

[24] M. Naguib, O. Mashtalir, J. Carle, V. Presser, J. Lu, L. Hultman, Y. Gogotsi, M. W. Barsoum, Two-dimensional transition metal carbides, ACS Nano 6 (2012) 1322–1331, https://doi.org/10.1021/nn204153h.

[25] Y. Guan, R. Zhao, Y.e. Cong, K. Chen, J. Wu, H. Zhu, Z. Dong, Q. Zhang, G. Yuan, Y. Li, J. Zhang, X. Li, Flexible Ti$_2$C MXene film: Synthesis, electrochemical performance and capacitance behavior, Chem. Eng. J. 433 (2022), 133582, https://doi.org/10.1016/j.cej.2021.133582.

[26] T. Wojciechowski, A. Rozmysłowska-Wojciechowska, G. Matyszczak, M. Wrzecionek, A. Olszyna, A. Peter, A. Mihaly-Cozmuta, C. Nicula, L. Mihaly-Cozmuta, S. Podsiadło, D. Basiak, W. Ziemkowska, A. Jastrzębska, Ti$_2$C MXene modified with ceramic oxide and noble metal nanoparticles: synthesis, morphostructural properties, and high photocatalytic activity, Inorg. Chem. 58 (11) (2019) 7602–7614.

[27] H. He, J. Wang, Q. Xia, L. Wang, Q. Hu, A. Zhou, Effect of electrolyte on supercapacitor performance of two-dimensional molybdenum carbide (Mo$_2$CTx) MXene prepared by hydrothermal etching, Appl. Surf. Sci. 568 (2021), 150971, https://doi.org/10.1016/j.apsusc.2021.150971.

[28] A.E. Ghazaly, W. Zheng, J. Halim, E.N. Tseng, P.OÅ. Persson, B. Ahmed, J. Rosen, Enhanced supercapacitive performance of Mo1. 33C MXene based asymmetric supercapacitors in lithium chloride electrolyte, Energy Storage Mater. 41 (2021) 203–208.

[29] J. Xiao, J. Wen, J. Zhao, X. Ma, H. Gao, X. Zhang, A safe etching route to synthesize highly crystalline Nb$_2$CTx MXene for high performance asymmetric supercapacitor applications, Electrochim. Acta. 337 (2020) 135803, https://doi.org/10.1016/j.electacta.2020.135803.

[30] J. Nan, X. Guo, J. Xiao, X. Li, W. Chen, W. Wu, H. Liu, Y. Wang, M. Wu, G. Wang, Nanoengineering of 2D MXene-based materials for energy storage applications, Small 17 (2021) 1902085, https://doi.org/10.1002/smll.201902085.

[31] J. Chen, J. Ren, H. Zhang, J. Qi, Y. Sui, F. Wei, Ni-Co-Fe layered double hydroxide coated on Ti3C2 MXene for high-performance asymmetric supercapacitor, Appl. Surf. Sci. 562 (2021), 150116, https://doi.org/10.1016/j.apsusc.2021.150116.

[32] Q.i. Yang, Z. Huang, X. Li, Z. Liu, H. Li, G. Liang, D. Wang, Q. Huang, S. Zhang, S. Chen, C. Zhi, others, A wholly degradable, rechargeable Zn-Ti$_3$C$_2$ MXene capacitor with superior anti-self-discharge function, ACS Nano 13 (7) (2019) 8275–8283.

[33] Q. Fan, R. Zhao, M. Yi, P. Qi, C. Chai, H. Ying, J. Hao, Ti$_3$C$_2$-MXene composite films functionalized with polypyrrole and ionic liquid-based microemulsion particles for supercapacitor applications, Chem. Eng. J. 428 (2022), 131107, https://doi.org/10.1016/j.cej.2021.131107.

[34] Y. Zhang, F. Li, Robust half-metallic ferromagnetism in Cr$_3$C$_2$ MXene, J. Magn. Magn. Mater. 433 (2017) 222–226, https://doi.org/10.1016/j.jmmm.2017.03.031.

[35] C. Li, J. Guo, J. Wang, D. Ma, B. Wang, Design of MXene contacts for high-performance WS$_2$ transistors, Appl. Surf. Sci. 527 (2020), 146701, https://doi.org/10.1016/j.apsusc.2020.146701.

[36] M. Ghidiu, M. Naguib, C. Shi, O. Mashtalir, L.M. Pan, B. Zhang, J. Yang, Y. Gogotsi, S.J.L. Billinge, M.W. Barsoum, Synthesis and characterization of two-dimensional Nb$_4$C$_3$ (MXene), Chem. Commun. 50 (2014) 9517–9520, https://doi.org/10.1039/C4CC03366C.

[37] T. Zhou, W. Zhao, K. Yang, Q. Yao, Y.i. Li, B. Wu, J. Liu, Atomic vacancy defect, Frenkel defect and transition metals (Sc, V, Zr) doping in Ti$_4$N$_3$ MXene nanosheet:

A first-principles investigation, Appl. Sci. 10 (2020) 2450, https://doi.org/10.3390/app10072450.

[38] H. Chen, D. Yang, Q. Zhang, S. Jin, L. Guo, J. Deng, X. Li, X. Chen, A Series of MAX Phases with MA-Triangular-Prism Bilayers and Elastic Properties, Angew, Chemie. 131 (2019) 4624–4628, https://doi.org/10.1002/ange.201814128.

[39] R. Meshkian, L.-Å. Näslund, J. Halim, J. Lu, M.W. Barsoum, J. Rosen, Synthesis of two-dimensional molybdenum carbide, Mo₂C, from the gallium based atomic laminate Mo₂Ga₂C, Scr. Mater. 108 (2015) 147–150, https://doi.org/10.1016/j.scriptamat.2015.07.003.

[40] J. Zhou, X. Zha, X. Zhou, F. Chen, G. Gao, S. Wang, C. Shen, T. Chen, C. Zhi, P. Eklund, S. Du, J. Xue, W. Shi, Z. Chai, Q. Huang, others, Synthesis and electrochemical properties of two-dimensional hafnium carbide, ACS Nano 11 (4) (2017) 3841–3850.

[41] B. Anasori, M.R. Lukatskaya, Y. Gogotsi, 2D metal carbides and nitrides (MXenes) for energy storage, Nat. Rev. Mater. 2 (2017) 1–17, https://doi.org/10.1038/natrevmats.2016.98.

[42] T. Qin, Z. Wang, Y. Wang, F. Besenbacher, M. Otyepka, M. Dong, Recent progress in emerging two-dimensional transition metal carbides, Nano-Micro Lett. 13 (2021) 1–34, https://doi.org/10.1007/s40820-021-00710-7.

[45] M. Kurtoglu, M. Naguib, Y. Gogotsi, M.W. Barsoum, First principles study of two-dimensional early transition metal carbides, Mrs Commun. 2 (2012) 133–137, https://doi.org/10.1557/mrc.2012.25.

[46] J. Liu, H.-B. Zhang, R. Sun, Y. Liu, Z. Liu, A. Zhou, Z.-Z. Yu, Hydrophobic, flexible, and lightweight MXene foams for high-performance electromagnetic-interference shielding, Adv. Mater. 29 (2017) 1702367, https://doi.org/10.1002/adma.201702367.

[47] Y. Zhu, S. Murali, W. Cai, X. Li, J.W. Suk, J.R. Potts, R.S. Ruoff, Graphene and graphene oxide: synthesis, properties, and applications, Adv. Mater. 22 (2010) 3906–3924, https://doi.org/10.1002/adma.201001068.

[48] L. Gao, C. Li, W. Huang, S. Mei, H. Lin, Q.i. Ou, Y.e. Zhang, J. Guo, F. Zhang, S. Xu, H. Zhang, others, MXene/polymer membranes: synthesis, properties, and emerging applications, Chem. Mater. 32 (5) (2020) 1703–1747.

[51] Y. Xie, M. Naguib, V.N. Mochalin, M.W. Barsoum, Y. Gogotsi, X. Yu, K.-W. Nam, X.-Q. Yang, A.I. Kolesnikov, P.R.C. Kent, Role of surface structure on Li-ion energy storage capacity of two-dimensional transition-metal carbides, J. Am. Chem. Soc. 136 (2014) 6385–6394, https://doi.org/10.1021/ja501520b.

[52] W. Feng, H. Luo, Y. Wang, S. Zeng, Y. Tan, H. Zhang, S. Peng, Ultrasonic assisted etching and delaminating of Ti₃C₂ Mxene, Ceram. Int. 44 (2018) 7084–7087, https://doi.org/10.1016/j.ceramint.2018.01.147.

[53] C. Zhan, M. Naguib, M. Lukatskaya, P.R.C. Kent, Y. Gogotsi, D. Jiang, Understanding the MXene pseudocapacitance, J. Phys. Chem. Lett. 9 (2018) 1223–1228, https://doi.org/10.1021/acs.jpclett.8b00200.

[54] X. Mu, D. Wang, F. Du, G. Chen, C. Wang, Y. Wei, Y. Gogotsi, Y. Gao, Y. Dall'Agnese, Revealing the pseudo-intercalation charge storage mechanism of MXenes in acidic electrolyte, Adv. Funct. Mater. 29 (2019) 1902953, https://doi.org/10.1002/adfm.201902953.

[55] A.C. Foucher, M. Han, C.E. Shuck, K. Maleski, Y. Gogotsi, E.A. Stach, Shifts in valence states in bimetallic MXenes revealed by electron energy-loss spectroscopy (EELS), 2D Mater. 9 (2) (2022) 025004.

[57] Y. Chae, S.J. Kim, S.-Y. Cho, J. Choi, K. Maleski, B.-J. Lee, H.-T. Jung, Y. Gogotsi, Y. Lee, C.W. Ahn, An investigation into the factors governing the oxidation of two-dimensional Ti₃C₂ MXene, Nanoscale 11 (2019) 8387–8393, https://doi.org/10.1039/C9NR00084D.

[58] C.J. Zhang, S. Pinilla, N. McEvoy, C.P. Cullen, B. Anasori, E. Long, S.-H. Park, A. Seral-Ascaso, A. Shmeliov, D. Krishnan, C. Morant, X. Liu, G.S. Duesberg, Y. Gogotsi, V. Nicolosi, others, Oxidation stability of colloidal two-dimensional titanium carbides (MXenes), Chem. Mater. 29 (11) (2017) 4848–4856.

[59] Y. Lee, S.J. Kim, Y.-J. Kim, Y. Lim, Y. Chae, B.-J. Lee, Y.-T. Kim, H. Han, Y. Gogotsi, C.W. Ahn, Oxidation-resistant titanium carbide MXene films, J. Mater. Chem. A. 8 (2020) 573–581, https://doi.org/10.1039/C9TA07036B.

[60] Z. Guo, J. Zhou, C. Si, Z. Sun, Flexible two-dimensional Ti n+1 C n (n= 1, 2 and 3) and their functionalized MXenes predicted by density functional theories, Phys. Chem. Chem. Phys. 17 (2015) 15348–15354, https://doi.org/10.1039/C5CP00775E.

[61] M. Khazaei, M. Arai, T. Sasaki, C.-Y. Chung, N.S. Venkataramanan, M. Estili, Y. Sakka, Y. Kawazoe, Novel electronic and magnetic properties of two-dimensional transition metal carbides and nitrides, Adv. Funct. Mater. 23 (2013) 2185–2192, https://doi.org/10.1002/adfm.201202502.

[62] N.J. Lane, M.W. Barsoum, J.M. Rondinelli, Correlation effects and spin-orbit interactions in two-dimensional hexagonal 5d transition metal carbides, Ta n+1 Cn (n = 1,2,3), EPL 101 (5) (2013) 57004.

[63] I.R. Shein, A.L. Ivanovskii, Graphene-like titanium carbides and nitrides Tin+ 1Cn, Tin+1Nn (n= 1, 2, and 3) from de-intercalated MAX phases: First-principles probing of their structural, electronic properties and relative stability, Comput. Mater. Sci. 65 (2012) 104–114, https://doi.org/10.1016/j.commatsci.2012.07.011.

[64] Y. Xie, P.R.C. Kent, Hybrid density functional study of structural and electronic properties of functionalized Ti n+ 1 X n (X= C, N) monolayers, Phys. Rev. B. 87 (2013), 235441, https://doi.org/10.1103/PhysRevB.87.235441.

[65] F. Shahzad, M. Alhabeb, C.B. Hatter, B. Anasori, S. Man Hong, C.M. Koo, Y. Gogotsi, Electromagnetic interference shielding with 2D transition metal carbides (MXenes), Science 353 (6304) (2016) 1137–1140.

[66] M. Naguib, V. Presser, D. Tallman, J. Lu, L. Hultman, Y. Gogotsi, M.W. Barsoum, Y. Zhou, On the topotactic transformation of Ti₂AlC into a Ti-C-O-F cubic phase by heating in molten lithium fluoride in air, J. Am. Ceram. Soc. 94 (12) (2011) 4556–4561.

[67] D. Wang, J. Si, S. Lin, R. Zhang, Y. Huang, J. Yang, W. Lu, X. Zhu, Y. Sun, Achieving macroscopic V₄C₃T x MXene by selectively etching Al from V₄AlC₃ single crystals, Inorg. Chem. 59 (2020) 3239–3248, https://doi.org/10.1021/acs.inorgchem.9b03625.

[68] Y. Dall'Agnese, P.-L. Taberna, Y. Gogotsi, P. Simon, Two-dimensional vanadium carbide (MXene) as positive electrode for sodium-ion capacitors, J. Phys. Chem. Lett. 6 (12) (2015) 2305–2309.

[71] L. Wang, H. Zhang, B. Wang, C. Shen, C. Zhang, Q. Hu, A. Zhou, B. Liu, Synthesis and electrochemical performance of Ti₃C₂Tx with hydrothermal process, Electron. Mater. Lett. 12 (2016) 702–710, https://doi.org/10.1007/s13391-016-6088-z.

[72] L.H. Karlsson, J. Birch, J. Halim, M.W. Barsoum, P.O.Å. Persson, Atomically resolved structural and chemical investigation of single MXene sheets, Nano Lett. 15 (2015) 4955–4960, https://doi.org/10.1021/acs.nanolett.5b00737.

[73] G. Li, L. Tan, Y. Zhang, B. Wu, L. Li, Highly efficiently delaminated single-layered MXene nanosheets with large lateral size, Langmuir 33 (2017) 9000–9006, https://doi.org/10.1021/acs.langmuir.7b01339.

[74] J. Halim, M.R. Lukatskaya, K.M. Cook, J. Lu, C.R. Smith, L.-Å. Näslund, S.J. May, L. Hultman, Y. Gogotsi, P. Eklund, M.W. Barsoum, others, Transparent conductive two-dimensional titanium carbide epitaxial thin films, Chem. Mater. 26 (7) (2014) 2374–2381.

[75] X. Xie, Y. Xue, L. Li, S. Chen, Y. Nie, W. Ding, Z. Wei, Surface Al leached Ti₃AlC₂ as a substitute for carbon for use as a catalyst support in a harsh corrosive electrochemical system, Nanoscale 6 (2014) 11035–11040, https://doi.org/10.1039/C4NR02080D.

[76] H.-J. Yan, Z. Li, S.-C. Liu, X. Wang, X. Zhang, D.-J. Xue, J.-S. Hu, Investigation of weak interlayer coupling in 2D layered GeS₂ from theory to experiment, Nano Res. 15 (2022) 1013–1019, https://doi.org/10.1007/s12274-021-3589-3.

[77] C.N.R. Rao, K.S. Subrahmanyam, H.S.S. Ramakrishna Matte, B. Abdulhakeem, A. Govindaraj, B. Das, P. Kumar, A. Ghosh, D.J. Late, A study of the synthetic methods and properties of graphenes, Sci. Technol. Adv. Mater. 11 (5) (2010) 054502.

[78] M. Naguib, M.W. Barsoum, Y. Gogotsi, Ten years of progress in the synthesis and development of MXenes, Adv. Mater. 33 (2021) 2103393, https://doi.org/10.1002/adma.202103393.

[79] M. Khazaei, M. Arai, T. Sasaki, M. Estili, Y. Sakka, Trends in electronic structures and structural properties of MAX phases: a first-principles study on M₂AlC (M= Sc, Ti, Cr, Zr, Nb, Mo, Hf, or Ta), M₂AlN, and hypothetical M₂AlB phases, J. Phys. Condens. Matter. 26 (50) (2014), 505503, https://doi.org/10.1088/0953-8984/26/50/505503.

[80] P. Srivastava, A. Mishra, H. Mizuseki, K.-R. Lee, A.K. Singh, Mechanistic insight into the chemical exfoliation and functionalization of Ti₃C₂ MXene, ACS Appl. Mater. & Interfaces 8 (2016) 24256–24264, https://doi.org/10.1021/acsami.6b08413.

[81] M. Alhabeb, K. Maleski, B. Anasori, P. Lelyukh, L. Clark, S. Sin, Y. Gogotsi, Guidelines for synthesis and processing of two-dimensional titanium carbide (Ti₃C₂T x MXene), Chem. Mater. 29 (2017) 7633–7644, https://doi.org/10.1021/acs.chemmater.7b02847.

[82] X. Su, J. Zhang, H. Mu, J. Zhao, Z. Wang, Z. Zhao, C. Han, Z. Ye, Effects of etching temperature and ball milling on the preparation and capacitance of Ti₃C₂ MXene, J. Alloys Compd. 752 (2018) 32–39, https://doi.org/10.1016/j.jallcom.2018.04.152.

[83] J. Guo, Q. Peng, H. Fu, G. Zou, Q. Zhang, Heavy-metal adsorption behavior of two-dimensional alkalization-intercalated MXene by first-principles calculations, J. Phys. Chem. C. 119 (2015) 20923–20930, https://doi.org/10.1021/acs.jpcc.5b05426.

[84] X. Guo, X. Zhang, S. Zhao, Q. Huang, J. Xue, High adsorption capacity of heavy metals on two-dimensional MXenes: an ab initio study with molecular dynamics simulation, Phys. Chem. Chem. Phys. 18 (2016) 228–233, https://doi.org/10.1039/C5CP06078H.

[85] B. Soundiraraju, B.K. George, Two-dimensional titanium nitride (Ti₂N) MXene: synthesis, characterization, and potential application as surface-enhanced Raman scattering substrate, ACS Nano 11 (2017) 8892–8900, https://doi.org/10.1021/acsnano.7b03129.

[86] F. Liu, A. Zhou, J. Chen, J. Jia, W. Zhou, L. Wang, Q. Hu, Preparation of Ti₃C₂ and Ti₂C MXenes by fluoride salts etching and methane adsorptive properties, Appl. Surf. Sci. 416 (2017) 781–789, https://doi.org/10.1016/j.apsusc.2017.04.239.

[87] M. Khazaei, A. Ranjbar, K. Esfarjani, D. Bogdanovski, R. Dronskowski, S. Yunoki, Insights into exfoliation possibility of MAX phases to MXenes, Phys. Chem. Chem. Phys. 20 (2018) 8579–8592, https://doi.org/10.1039/C7CP08645H.

[88] B. Zhang, J. Zhu, P. Shi, W. Wu, F. Wang, Fluoride-free synthesis and microstructure evolution of novel two-dimensional Ti₃C₂(OH)₂ nanoribbons as high-performance anode materials for lithium-ion batteries, Ceram. Int. 45 (2019) 8395–8405, https://doi.org/10.1016/j.ceramint.2019.01.148.

[89] J. Wu, Y. Wang, Y. Zhang, H. Meng, Y. Xu, Y. Han, Z. Wang, Y. Dong, X. Zhang, Highly safe and ionothermal synthesis of Ti₃C₂ MXene with expanded interlayer spacing for enhanced lithium storage, J. Energy Chem. 47 (2020) 203–209, https://doi.org/10.1016/j.jechem.2019.11.029.

[90] X. Wang, H. Li, H. Li, S. Lin, W. Ding, X. Zhu, Z. Sheng, H. Wang, X. Zhu, Y. Sun, 2D/2D 1T-MoS₂/Ti₃C₂ MXene heterostructure with excellent supercapacitor performance, Adv. Funct. Mater. 30 (15) (2020), 190302, https://doi.org/10.1002/adfm.201910302.

[91] A.S. Levitt, M. Alhabeb, C.B. Hatter, A. Sarycheva, G. Dion, Y. Gogotsi, Electrospun MXene/carbon nanofibers as supercapacitor electrodes, J. Mater. Chem. A. 7 (2019) 269–277, https://doi.org/10.1039/C8TA09810G.

[92] T. Li, L. Yao, Q. Liu, J. Gu, R. Luo, J. Li, X. Yan, W. Wang, P. Liu, B. Chen, W. Zhang, W. Abbas, R. Naz, D.i. Zhang, others, Fluorine-free synthesis of high-purity $Ti_3C_2T_x$ (T= OH, O) via alkali treatment, Angew. Chemie Int. Ed. 57 (21) (2018) 6115–6119.

[93] J. Zhang, S. Seyedin, S.i. Qin, Z. Wang, S. Moradi, F. Yang, P.A. Lynch, W. Yang, J. Liu, X. Wang, J.M. Razal, others, Highly conductive $Ti_3C_2T_x$ MXene hybrid fibers for flexible and elastic fiber-shaped supercapacitors, Small 15 (8) (2019) 1804732.

[94] M. Ghidiu, M.R. Lukatskaya, M.-Q. Zhao, Y. Gogotsi, M.W. Barsoum, Conductive two-dimensional titanium carbide 'clay' with high volumetric capacitance, Nature 516 (2014) 78–81, https://doi.org/10.1038/nature13970.

[97] S. Yang, P. Zhang, F. Wang, A.G. Ricciardulli, M.R. Lohe, P.W.M. Blom, X. Feng, Fluoride-free synthesis of two-dimensional titanium carbide (MXene) using a binary aqueous system, Angew. Chemie. 130 (2018) 15717–15721, https://doi.org/10.1002/ange.201809662.

[98] T. Yin, Y. Li, R. Wang, O.A. Al-Hartomy, A. Al-Ghamdi, S. Wageh, X. Luo, X. Tang, H. Zhang, Synthesis of $Ti_3C_2F_x$ MXene with controllable fluorination by electrochemical etching for lithium-ion batteries applications, Ceram. Int. 47 (2021) 28642–28649, https://doi.org/10.1016/j.ceramint.2021.07.023.

[99] W. Sun, S.A. Shah, Y. Chen, Z. Tan, H. Gao, T. Habib, M. Radovic, M.J. Green, Electrochemical etching of Ti_2AlC to Ti_2CT_x (MXene) in low-concentration hydrochloric acid solution, J. Mater. Chem. A. 5 (2017) 21663–21668, https://doi.org/10.1039/C7TA05574A.

[100] M.R. Lukatskaya, J. Halim, B. Dyatkin, M. Naguib, Y.S. Buranova, M. W. Barsoum, Y. Gogotsi, Room-temperature carbide-derived carbon synthesis by electrochemical etching of MAX phases, Angew. Chemie. 126 (2014) 4977–4980, https://doi.org/10.1002/ange.201402513.

[101] S.-Y. Pang, Y.-T. Wong, S. Yuan, Y. Liu, M.-K. Tsang, Z. Yang, H. Huang, W.-T. Wong, J. Hao, Universal strategy for HF-free facile and rapid synthesis of two-dimensional MXenes as multifunctional energy materials, J. Am. Chem. Soc. 141 (2019) 9610–9616, https://doi.org/10.1021/jacs.9b02578.

[102] N. Thakur, P. Kumar, D.C. Sati, R. Neffati, P. Sharma, Recent advances in two-dimensional MXenes for power and smart energy systems, J. Energy Storage. 50 (2022), 104604, https://doi.org/10.1016/j.est.2022.104604.

[103] A. Heidarpour, M. Faraji, A. Haghighi, Production and characterization of carbide-derived-nanocarbon structures obtained by HF electrochemical etching of Ti_3AlC_2, Ceram. Int. 48 (8) (2022) 11466–11474.

[104] C. Zhou, X. Zhao, Y. Xiong, Y. Tang, X. Ma, Q. Tao, C. Sun, W. Xu, A review of etching methods of MXene and applications of MXene conductive hydrogels, Eur. Polym. J. 167 (2022), 111063, https://doi.org/10.1016/j.eurpolymj.2022.111063.

[105] Y. Cao, C. Guo, Y. Zou, Rapid synthesis of MXenes at room temperature, Mater. Sci. Technol. 35 (2019) 1904–1907, https://doi.org/10.1080/02670836.2019.1654250.

[106] L. Zhao, Z. Wang, Y. Li, S. Wang, L. Wang, Z. Qi, Q. Ge, X. Liu, J.Z. Zhang, Designed synthesis of chlorine and nitrogen co-doped Ti_3C_2 MXene quantum dots and their outstanding hydroxyl radical scavenging properties, J. Mater. Sci. & Technol. 78 (2021) 30–37, https://doi.org/10.1016/j.jmst.2020.10.048.

[107] Y.J. Mai, Y.G. Li, S.L. Li, L.Y. Zhang, C.S. Liu, X.H. Jie, Self-lubricating Ti_3C_2 nanosheets/copper composite coatings, J. Alloys Compd. 770 (2019) 1–5, https://doi.org/10.1016/j.jallcom.2018.08.100.

[108] L.-Y. Xiu, Z.-Y. Wang, J.-S. Qiu, General synthesis of MXene by green etching chemistry of fluoride-free Lewis acidic melts, Rare Met. 39 (2020) 1237–1238, https://doi.org/10.1007/s12598-020-01488-0.

[109] W. Meng, X. Liu, H. Song, Y. Xie, X. Shi, M. Dargusch, Z.-G. Chen, Z. Tang, S. Lu, Advances and challenges in 2D MXenes: From structures to energy storage and conversions, Nano Today 40 (2021), 101273, https://doi.org/10.1016/j.nantod.2021.101273.

[110] H. Jin, Q. Gu, B. Chen, C. Tang, Y. Zheng, H. Zhang, M. Jaroniec, S.-Z. Qiao, Molten salt-directed catalytic synthesis of 2D layered transition-metal nitrides for efficient hydrogen evolution, Chem 6 (2020) 2382–2394, https://doi.org/10.1016/j.chempr.2020.06.037.

[111] X. Liu, N. Fechler, M. Antonietti, Salt melt synthesis of ceramics, semiconductors and carbon nanostructures, Chem. Soc. Rev. 42 (2013) 8237–8265, https://doi.org/10.1039/C3CS60159E.

[112] L. Huang, Z. Hu, H. Jin, J. Wu, K. Liu, Z. Xu, J. Wan, H.e. Zhou, J. Duan, B. Hu, J. Zhou, others, Salt-assisted synthesis of 2D materials, Adv. Funct. Mater. 30 (19) (2020) 1908486.

[113] L. Shi, K. Chen, R. Du, A. Bachmatiuk, M.H. Rümmeli, M.K. Priydarshi, Y. Zhang, A. Manivannan, Z. Liu, Direct synthesis of few-layer graphene on NaCl crystals, Small 11 (2015) 6302–6308, https://doi.org/10.1002/smll.201502013.

[114] Z. Hu, X.u. Xiao, H. Jin, T. Li, M. Chen, Z. Liang, Z. Guo, J. Li, J. Wan, L. Huang, Y. Zhang, G. Feng, J. Zhou, others, Rapid mass production of two-dimensional metal oxides and hydroxides via the molten salts method, Nat. Commun. 8 (1) (2017), https://doi.org/10.1038/ncomms15630.

[115] A. Djire, P. Pande, A. Deb, J.B. Siegel, O.T. Ajenifujah, L. He, A.E. Sleightholme, P. G. Rasmussen, L.T. Thompson, Unveiling the pseudocapacitive charge storage mechanisms of nanostructured vanadium nitrides using in-situ analyses, Nano Energy 60 (2019) 72–81, https://doi.org/10.1016/j.nanoen.2019.03.003.

[116] H. Jin, Z. Hu, T. Li, L. Huang, J. Wan, G. Xue, J. Zhou, Mass production of high-quality transition metal dichalcogenides nanosheets via a molten salt method, Adv. Funct. Mater. 29 (2019) 1900649, https://doi.org/10.1002/adfm.201900649.

[117] K.H. Yoon, Y.S. Cho, D.H. Kang, Molten salt synthesis of lead-based relaxors, J. Mater. Sci. 33 (1998) 2977–2984, https://doi.org/10.1023/A:1004310931643.

[118] P. Urbankowski, B. Anasori, T. Makaryan, D. Er, S. Kota, P.L. Walsh, M. Zhao, V. B. Shenoy, M.W. Barsoum, Y. Gogotsi, Synthesis of two-dimensional titanium nitride Ti 4 N 3 (MXene), Nanoscale 8 (2016) 11385–11391, https://doi.org/10.1039/C6NR02253G.

[119] K. Arole, J.W. Blivin, S. Saha, D.E. Holta, X. Zhao, A. Sarmah, H. Cao, M. Radovic, J.L. Lutkenhaus, M.J. Green, Water-dispersible $Ti_3C_2T_z$ MXene nanosheets by molten salt etching, Iscience. 24 (12) (2021), 103403, https://doi.org/10.1016/j.isci.2021.103403.

[120] L. Guo, W.-Y. Jiang, M. Shen, C. Xu, C.-X. Ding, S.-F. Zhao, T.-T. Yuan, C.-Y. Wang, X.-Q. Zhang, J.-Q. Wang, High capacitance of MXene (Ti_3C_2Tx) through Intercalation and Surface Modification in Molten Salt, Electrochim. Acta. 401 (2022), 139476, https://doi.org/10.1016/j.electacta.2021.139476.

[121] R. Adalati, M. Sharma, S. Sharma, A. Kumar, G. Malik, R. Boukherroub, R. Chandra, Metal nitrides as efficient electrode material for supercapacitors: A review, J. Energy Storage. 56 (2022), 105912, https://doi.org/10.1016/j.est.2022.105912.

[122] M. Li, J. Lu, K. Luo, Y. Li, K. Chang, K.e. Chen, J. Zhou, J. Rosen, L. Hultman, P. Eklund, P.O.Å. Persson, S. Du, Z. Chai, Z. Huang, Q. Huang, others, Element replacement approach by reaction with Lewis acidic molten salts to synthesize nanolaminated MAX phases and MXenes, J. Am. Chem. Soc. 141 (11) (2019) 4730–4737.

[124] Y. Li, H. Shao, Z. Lin, J. Lu, L. Liu, B. Duployer, P.O.Å. Persson, P. Eklund, L. Hultman, M. Li, K.e. Chen, X.-H. Zha, S. Du, P. Rozier, Z. Chai, E. Raymundo-Piñero, P.-L. Taberna, P. Simon, Q. Huang, A general Lewis acidic etching route for preparing MXenes with enhanced electrochemical performance in non-aqueous electrolyte, Nat. Mater. 19 (8) (2020) 894–899.

[125] Z. Bao, C. Lu, X. Cao, P. Zhang, L.i. Yang, H. Zhang, D. Sha, W. He, W. Zhang, L. Pan, Z. Sun, others, Role of MXene surface terminations in electrochemical energy storage: A review, Chinese Chem. Lett. 32 (9) (2021) 2648–2658.

[126] V. Kamysbayev, A.S. Filatov, H. Hu, X. Rui, F. Lagunas, D. Wang, R.F. Klie, D. V. Talapin, Covalent surface modifications and superconductivity of two-dimensional metal carbide MXenes, Science (80-.). 369 (2020) 979–983, https://doi.org/10.1126/science.aba8311.

[127] R. Luo, R. Li, C. Jiang, R. Qi, M. Liu, C. Luo, H. Lin, R. Huang, H. Peng, Facile synthesis of cobalt modified 2D titanium carbide with enhanced hydrogen evolution performance in alkaline media, Int. J. Hydrogen Energy. 46 (2021) 32536–32545, https://doi.org/10.1016/j.ijhydene.2021.07.110.

[128] H. Zeng, L. Deng, L. Yang, H. Wu, H. Zhang, C. Zhou, B. Liu, Z. Shi, Novel Prussian blue analogues@ MXene nanocomposite as heterogeneous activator of peroxymonosulfate for the degradation of coumarin: The nonnegligible role of Lewis-acid sites on MXene, Chem. Eng. J. 416 (2021), 128071, https://doi.org/10.1016/j.cej.2020.128071.

[129] U. Khan, Y. Luo, L.B. Kong, W. Que, Synthesis of fluorine free MXene through lewis acidic etching for application as electrode of proton supercapacitors, J. Alloys Compd. 926 (2022), 166903, https://doi.org/10.1016/j.jallcom.2022.166903.

[130] X. Liang, J. Yun, K. Xu, H. Xiang, Y. Wang, Y. Sun, Y. Yu, A multi-layered Ti_3C_2/Li_2S composite as cathode material for advanced lithium-sulfur batteries, J. Energy Chem. 39 (2019) 176–181, https://doi.org/10.1016/j.jechem.2019.02.002.

[131] X. Liang, A. Garsuch, L.F. Nazar, Sulfur cathodes based on conductive MXene nanosheets for high-performance lithium–sulfur batteries, Angew. Chemie. 127 (2015) 3979–3983, https://doi.org/10.1002/ange.201410174.

[132] X. Zhao, M. Liu, Y. Chen, B. Hou, N. Zhang, B. Chen, N. Yang, K. Chen, J. Li, L. An, Fabrication of layered Ti_3C_2 with an accordion-like structure as a potential cathode material for high performance lithium–sulfur batteries, J. Mater. Chem. A. 3 (2015) 7870–7876, https://doi.org/10.1039/C4TA07101H.

[133] Z. Zhang, Q. Yan, Z. Liu, X. Zhao, Z. Wang, J. Sun, Z.L. Wang, R. Wang, L. Li, Flexible MXene composed triboelectric nanogenerator via facile vacuum-assistant filtration method for self-powered biomechanical sensing, Nano Energy 88 (2021), 106257, https://doi.org/10.1016/j.nanoen.2021.106257.

[134] X. Zheng, Q. Hu, Z. Wang, W. Nie, P. Wang, C. Li, Roll-to-roll layer-by-layer assembly bark-shaped carbon nanotube/Ti_3C_2Tx MXene textiles for wearable electronics, J. Colloid Interface Sci. 602 (2021) 680–688, https://doi.org/10.1016/j.jcis.2021.06.043.

[135] M. Zhang, Y. Wang, F. Gao, Y.u. Wang, X. Shen, N. He, J. Zhu, Y. Chen, X. Wan, X. Lian, E. Hu, J. Xu, Y.i. Tong, others, Formation of new MXene film using spinning coating method with DMSO solution and its application in advanced memristive device, Ceram. Int. 45 (15) (2019) 19467–19472.

[136] S.-H. Seok, S. Choo, J. Kwak, H. Ju, J.-H. Han, W.-S. Kang, J. Lee, S.-Y. Kim, D. H. Lee, J. Lee, J. Wang, S. Song, W. Jo, B.M. Jung, H.G. Chae, J.S. Son, S.-Y. Kwon, others, Synthesis of high quality 2D carbide MXene flakes using a highly purified MAX precursor for ink applications, Nanoscale Adv. 3 (2) (2021) 517–527.

[137] X. Zheng, J. Shen, Q. Hu, W. Nie, Z. Wang, L. Zou, C. Li, Vapor phase polymerized conducting polymer/MXene textiles for wearable electronics, Nanoscale 13 (2021) 1832–1841, https://doi.org/10.1039/D0NR07433K.

[138] Y.-L. Huang, S.-W. Bian, Vacuum-filtration assisted layer-by-layer strategy to design MXene/carbon nanotube@ MnO_2 all-in-one supercapacitors, J. Mater. Chem. A. 9 (2021) 21347–21356, https://doi.org/10.1039/D1TA06089A.

[139] Y. Tian, Y. An, J. Feng, Flexible and freestanding silicon/MXene composite papers for high-performance lithium-ion batteries, ACS Appl. Mater. & Interfaces. 11 (2019) 10004–10011, https://doi.org/10.1021/acsami.8b21893.

[140] W. Yang, J.J. Byun, J. Yang, F.P. Moissinac, Y. Ma, H. Ding, W. Sun, R.A.W. Dryfe, S. Barg, All-in-one MXene-boron nitride-MXene "OREO" with vertically aligned

channels for flexible structural supercapacitor design, ACS Appl. Energy Mater. 4 (2021) 7959–7972, https://doi.org/10.1021/acsaem.1c01240.

[141] L. Qin, J. Jiang, Q. Tao, C. Wang, I. Persson, M. Fahlman, P.O.Å. Persson, L. Hou, J. Rosen, F. Zhang, A flexible semitransparent photovoltaic supercapacitor based on water-processed MXene electrodes, J. Mater. Chem. A. 8 (11) (2020) 5467–5475.

[142] L. Li, J. Fu, Y.-R. Cho, J.M. Yun, Y.S. Jung, S.H. Kwon, K.H. Kim, Hierarchically layered nanocomposite electrodes formed by spray-injected MXene nanosheets for ultrahigh-performance flexible supercapacitors, Appl. Surf. Sci. 549 (2021), 149226, https://doi.org/10.1016/j.apsusc.2021.149226.

[143] C. Xu, L. Wang, Z. Liu, L. Chen, J. Guo, N. Kang, X.-L. Ma, H.-M. Cheng, W. Ren, Large-area high-quality 2D ultrathin Mo$_2$C superconducting crystals, Nat. Mater. 14 (2015) 1135–1141, https://doi.org/10.1038/nmat4374.

[144] Y. Liu, J. Yu, D. Guo, Z. Li, Y. Su, Ti$_3$C$_2$Tx MXene/graphene nanocomposites: Synthesis and application in electrochemical energy storage, J. Alloys Compd. 815 (2020), 152403, https://doi.org/10.1016/j.jallcom.2019.152403.

[145] P. Forouzandeh, S.C. Pillai, MXenes-based nanocomposites for supercapacitor applications, Curr. Opin. Chem. Eng. 33 (2021), 100710, https://doi.org/10.1016/j.coche.2021.100710.

[146] T. Brousse, D. Bélanger, J.W. Long, To be or not to be pseudocapacitive? J. Electrochem. Soc. 162 (5) (2015) A5185–A5189.

[147] Y. Gogotsi, R.M. Penner, Energy storage in nanomaterials–capacitive, pseudocapacitive, or battery-like? ACS Nano 12 (2018) 2081–2083, https://doi.org/10.1021/acsnano.8b01914.

[148] S. Panda, K. Deshmukh, S.K.K. Pasha, J. Theerthagiri, S. Manickam, M.Y. Choi, MXene based emerging materials for supercapacitor applications: Recent advances, challenges, and future perspectives, Coord. Chem. Rev. 462 (2022), 214518, https://doi.org/10.1016/j.ccr.2022.214518.

[149] M.R. Lukatskaya, O. Mashtalir, C.E. Ren, Y. Dall'Agnese, P. Rozier, P.L. Taberna, M. Naguib, P. Simon, M.W. Barsoum, Y. Gogotsi, Cation intercalation and high volumetric capacitance of two-dimensional titanium carbide, Science 341 (6153) (2013) 1502–1505.

[150] M.D. Levi, M.R. Lukatskaya, S. Sigalov, N. Beidaghi, N. Shpigel, L. Daikhin, D. Aurbach, M.W. Barsoum, Y. Gogotsi, Solving the capacitive paradox of 2D MXene using electrochemical quartz-crystal admittance and in situ electronic conductance measurements, Adv. Energy Mater. 5 (2015) 1400815, https://doi.org/10.1002/aenm.201400815.

[151] M. Ghidiu, S. Kota, J. Halim, A.W. Sherwood, N. Nedfors, J. Rosen, V. N. Mochalin, M.W. Barsoum, Alkylammonium cation intercalation into Ti$_3$C$_2$ (MXene): effects on properties and ion-exchange capacity estimation, Chem. Mater. 29 (2017) 1099–1106, https://doi.org/10.1021/acs.chemmater.6b04234.

[152] A. Sohan, P. Banoth, M. Aleksandrova, A. Nirmala Grace, P. Kollu, Review on MXene synthesis, properties, and recent research exploring electrode architecture for supercapacitor applications, Int. J. Energy Res. 45 (2021) 19746–19771, https://doi.org/10.1002/er.7068.

[153] A. Sugahara, Y. Ando, S. Kajiyama, K. Yazawa, K. Gotoh, M. Otani, M. Okubo, A. Yamada, Negative dielectric constant of water confined in nanosheets, Nat. Commun. 10 (2019) 1–7, https://doi.org/10.1038/s41467-019-08789-8.

[154] H. Huang, X. Chu, Y. Xie, B. Zhang, Z. Wang, Z. Duan, N. Chen, Z. Xu, H. Zhang, W. Yang, Ti$_3$C$_2$T$_x$ MXene-based micro-supercapacitors with ultrahigh volumetric energy density for all-in-one Si-electronics, ACS Nano 16 (2022) 3776–3784, https://doi.org/10.1021/acsnano.1c08172.

[155] M. Hu, Z. Li, G. Li, T. Hu, C. Zhang, X. Wang, All-solid-state flexible fiber-based MXene supercapacitors, Adv. Mater. Technol. 2 (2017) 1700143, https://doi.org/10.1002/admt.201700143.

[156] Y. Wang, X. Wang, X. Li, Y. Bai, H. Xiao, Y. Liu, R. Liu, G. Yuan, Engineering 3D ion transport channels for flexible MXene films with superior capacitive performance, Adv. Funct. Mater. 29 (2019) 1900326, https://doi.org/10.1002/adfm.201900326.

[157] M. Guo, C. Liu, Z. Zhang, J. Zhou, Y. Tang, S. Luo, Flexible Ti$_3$C$_2$Tx/Al electrodes with ultrahigh areal capacitance: in situ regulation of interlayer conductivity and spacing, Adv. Funct. Mater. 28 (2018) 1803196, https://doi.org/10.1002/adfm.201803196.

[158] J. Shen, X. Li, L. Wan, K. Liang, B.K. Tay, L. Kong, X. Yan, An asymmetric supercapacitor with both ultra-high gravimetric and volumetric energy density based on 3D Ni(OH)$_2$/MnO$_2$@ carbon nanotube and activated polyaniline-derived carbon, ACS Appl. Mater. & Interfaces. 9 (2017) 668–676, https://doi.org/10.1021/acsami.6b12370.

[159] M.R. Lukatskaya, S. Kota, Z. Lin, M.-Q. Zhao, N. Shpigel, M.D. Levi, J. Halim, P.-L. Taberna, M.W. Barsoum, P. Simon, others, Ultra-high-rate pseudocapacitive energy storage in two-dimensional transition metal carbides, Nat. Energy. 2 (2017) 1–6, https://doi.org/10.1038/nenergy.2017.105.

[160] Z. Lin, D. Barbara, P.-L. Taberna, K.L. Van Aken, B. Anasori, Y. Gogotsi, P. Simon, Capacitance of Ti$_3$C$_2$Tx MXene in ionic liquid electrolyte, J. Power Sources. 326 (2016) 575–579, https://doi.org/10.1016/j.jpowsour.2016.04.035.

[161] Z. Lin, P. Rozier, B. Duployer, P.-L. Taberna, B. Anasori, Y. Gogotsi, P. Simon, Electrochemical and in-situ X-ray diffraction studies of Ti$_3$C$_2$ MXene in ionic liquid electrolyte, Electrochem. Commun. 72 (2016) 50–53, https://doi.org/10.1016/j.elecom.2016.08.023.

[162] K. Li, X. Wang, X. Wang, M. Liang, V. Nicolosi, Y. Xu, Y. Gogotsi, All-pseudocapacitive asymmetric MXene-carbon-conducting polymer supercapacitors, Nano Energy 75 (2020), 104971, https://doi.org/10.1016/j.nanoen.2020.104971.

[163] Y. Wei, M. Zheng, W. Luo, B. Dai, J. Ren, M. Ma, T. Li, Y. Ma, All pseudocapacitive MXene-MnO$_2$ flexible asymmetric supercapacitor, J. Energy Storage. 45 (2022), 103715, https://doi.org/10.1016/j.est.2021.103715.

[164] K. Maleski, V.N. Mochalin, Y. Gogotsi, Dispersions of two-dimensional titanium carbide MXene in organic solvents, Chem. Mater. 29 (2017) 1632–1640, https://doi.org/10.1021/acs.chemmater.6b04830.

[165] R. Ma, T. Sasaki, Two-dimensional oxide and hydroxide nanosheets: controllable high-quality exfoliation, molecular assembly, and exploration of functionality, Acc. Chem. Res. 48 (2015) 136–143, https://doi.org/10.1021/ar500311w.

[166] M. Boota, M. Pasini, F. Galeotti, W. Porzio, M.-Q. Zhao, J. Halim, Y. Gogotsi, Interaction of polar and nonpolar polyfluorenes with layers of two-dimensional titanium carbide (MXene): intercalation and pseudocapacitance, Chem. Mater. 29 (2017) 2731–2738, https://doi.org/10.1021/acs.chemmater.6b00933.

[167] A.K. Tomar, T. Kshetri, N.H. Kim, J.H. Lee, Cation and anion (de) intercalation into MXene/Perovskite oxides for high-rate intercalation pseudocapacitance, Energy Storage Mater. 50 (2022) 86–95, https://doi.org/10.1016/j.ensm.2022.05.012.

[168] F. Yang, D. Hegh, D. Song, J. Zhang, K.A.S. Usman, Z. Wang, P. Zhang, W. Ma, W. Yang, S.i. Qin, J.M. Razal, others, A nitrogenous pre-intercalation strategy for the synthesis of nitrogen-doped Ti$_3$C$_2$T$_x$ MXene with enhanced electrochemical capacitance, J. Mater. Chem. A. 9 (10) (2021) 6393–6401.

[169] W. Huang, L. Hu, Y. Tang, Z. Xie, H. Zhang, Recent advances in functional 2D Mxene-based nanostructures for next-generation devices, Adv. Funct. Mater. 30 (2020) 2005223, https://doi.org/10.1002/adfm.202005223.

[170] C. Lu, L. Yang, B. Yan, L. Sun, P. Zhang, W. Zhang, Z. Sun, Nitrogen-doped Ti$_3$C$_2$ MXene: mechanism investigation and electrochemical analysis, Adv. Funct. Mater. 30 (2020) 2000852, https://doi.org/10.1002/adfm.202000852.

[171] P. Komen, L. Ngamwongwan, S. Jungthawan, A. Junkaew, S. Suthirakun, Promoting Electrochemical Performance of Ti$_3$C$_2$O$_2$ MXene-Based Electrodes of Alkali-Ion Batteries via S Doping: Theoretical Insight, ACS Appl. Mater. & Interfaces. 13 (2021) 57306–57316, https://doi.org/10.1021/acsami.1c17802.

[172] Y. Wen, R. Li, J. Liu, Z. Wei, S. Li, L. Du, K. Zu, Z. Li, Y. Pan, H. Hu, A temperature-dependent phosphorus doping on Ti$_3$C$_2$Tx MXene for enhanced supercapacitance, J. Colloid Interface Sci. 604 (2021) 239–247, https://doi.org/10.1016/j.jcis.2021.06.020.

[173] R. Liu, W. Cao, D. Han, Y. Mo, H. Zeng, H. Yang, W. Li, Nitrogen-doped Nb$_2$CTx MXene as anode materials for lithium ion batteries, J. Alloys Compd. 793 (2019) 505–511, https://doi.org/10.1016/j.jallcom.2019.03.209.

[174] Z.-W. Gao, W. Zheng, L.Y.S. Lee, Highly Enhanced Pseudocapacitive Performance of Vanadium-Doped MXenes in Neutral Electrolytes, Small 15 (2019) 1902649, https://doi.org/10.1002/smll.201902649.

[175] H. Tang, R. Wang, L. Shi, E. Sheremet, R.D. Rodriguez, J. Sun, Post-processing strategies for improving the electrical and mechanical properties of MXenes, Chem. Eng. J. 425 (2021), 131472, https://doi.org/10.1016/j.cej.2021.131472.

[176] C. Yang, Y.i. Tang, Y. Tian, Y. Luo, M. Faraz Ud Din, X. Yin, W. Que, Flexible nitrogen-doped 2D titanium carbides (MXene) films constructed by an ex situ solvothermal method with extraordinary volumetric capacitance, Adv. Energy Mater. 8 (31) (2018) 1802087, https://doi.org/10.1002/aenm.201802087.

[178] H. Jiang, Z. Wang, L. Dong, M. Dong, Co(OH)$_2$/MXene composites for tunable pseudo-capacitance energy storage, Electrochim. Acta. 353 (2020), 136607, https://doi.org/10.1016/j.electacta.2020.136607.

[179] C. Sun, P. Zuo, W. Sun, R. Xia, Z. Dong, L. Zhu, J. Lv, G. Deng, L. Tan, Y. Dai, Self-assembly of alternating stacked 2D/2D Ti$_3$C$_2$Tx MXene/ZnMnNi LDH van der Waals heterostructures with ultrahigh supercapacitive performance, ACS Appl. Energy Mater. 3 (2020) 10242–10254, https://doi.org/10.1021/acsaem.0c02077.

[180] J. Lin, Y. Yu, Z. Zhang, F. Gao, S. Liu, W. Wang, G. Li, A novel approach for achieving high-efficiency photoelectrochemical water oxidation in InGaN Nanorods grown on Si system: MXene nanosheets as multifunctional interfacial modifier, Adv. Funct. Mater. 30 (2020) 1910479, https://doi.org/10.1002/adfm.201910479.

[181] Z. Wang, Y. Chen, M. Yao, J. Dong, Q. Zhang, L. Zhang, X. Zhao, Facile fabrication of flexible rGO/MXene hybrid fiber-like electrode with high volumetric capacitance, J. Power Sources. 448 (2020), 227398, https://doi.org/10.1016/j.jpowsour.2019.227398.

[182] M. Hu, C. Cui, C. Shi, Z.-S. Wu, J. Yang, R. Cheng, T. Guang, H. Wang, H. Lu, X. Wang, High-energy-density hydrogen-ion-rocking-chair hybrid supercapacitors based on Ti$_3$C$_2$Tx MXene and carbon nanotubes mediated by redox active molecule, ACS Nano 13 (2019) 6899–6905, https://doi.org/10.1021/acsnano.9b01762.

[183] Y. Yang, Z. Zeng, G. Zeng, D. Huang, R. Xiao, C. Zhang, C. Zhou, W. Xiong, W. Wang, M. Cheng, W. Xue, H. Guo, X. Tang, D. He, others, Ti$_3$C$_2$ Mxene/porous g-C$_3$N$_4$ interfacial Schottky junction for boosting spatial charge separation in photocatalytic H$_2$O$_2$ production, Appl. Catal. B Environ. 258 (2019), 117956, https://doi.org/10.1016/j.apcatb.2019.117956.

[184] J. Zhang, D. Jiang, L. Liao, L. Cui, R. Zheng, J. Liu, Ti$_3$C$_2$Tx MXene based hybrid electrodes for wearable supercapacitors with varied deformation capabilities, Chem. Eng. J. 429 (2022), 132232, https://doi.org/10.1016/j.cej.2021.132232.

[185] W. Zheng, J. Halim, A. El Ghazaly, A.S. Etman, E.N. Tseng, P.O.Å. Persson, J. Rosen, M.W. Barsoum, Flexible free-standing MoO$_3$/Ti$_3$C$_2$Tz MXene composite Films with high gravimetric and volumetric capacities, Adv. Sci. 8 (3) (2021) 2003656, https://doi.org/10.1002/advs.202003656.

[186] F. Li, Y.-L. Liu, G.-G. Wang, H.-Y. Zhang, B. Zhang, G.-Z. Li, Z.-P. Wu, L.-Y. Dang, J.-C. Han, Few-layered Ti$_3$C$_2$Tx MXenes coupled with Fe$_2$O$_3$ nanorod arrays grown on carbon cloth as anodes for flexible asymmetric supercapacitors, J. Mater. Chem. A. 7 (2019) 22631–22641, https://doi.org/10.1039/C9TA08144E.

[187] F. Mo, Q. Zhou, Q.i. Wang, Z. Hou, J. Wang, The applications of MOFs related materials in photo/electrochemical decontamination: An updated review, Chem. Eng. J. 450 (2022), 138326, https://doi.org/10.1016/j.cej.2022.138326.

[188] W. Xie, Y. Wang, J. Zhou, M. Zhang, J. Yu, C. Zhu, J. Xu, MOF-derived CoFe$_2$O$_4$ nanorods anchored in MXene nanosheets for all pseudocapacitive flexible supercapacitors with superior energy storage, Appl. Surf. Sci. 534 (2020), 147584, https://doi.org/10.1016/j.apsusc.2020.147584.

[189] X. Chen, P. Wang, Z. Feng, C. Meng, Y. Zhang, Conductive polymer intercalated vanadium oxide on carbon cloth for fast ammonium-ion storage in supercapacitor applications, Chem. Eng. J. 445 (2022), 136747, https://doi.org/10.1016/j.cej.2022.136747.

[190] Z. Ling, C.E. Ren, M.-Q. Zhao, J. Yang, J.M. Giammarco, J. Qiu, M.W. Barsoum, Y. Gogotsi, Flexible and conductive MXene films and nanocomposites with high capacitance, Proc. Natl. Acad. Sci. 111 (2014) 16676–16681, https://doi.org/10.1073/pnas.1414215111.

[191] J. Li, X. Yuan, C. Lin, Y. Yang, L. Xu, X. Du, J. Xie, J. Lin, J. Sun, Achieving high pseudocapacitance of 2D titanium carbide (MXene) by cation intercalation and surface modification, Adv. Energy Mater. 7 (2017) 1602725, https://doi.org/10.1002/aenm.201602725.

[192] C. Zhu, F. Geng, Macroscopic MXene ribbon with oriented sheet stacking for high-performance flexible supercapacitors, Carbon Energy 3 (2021) 142–152, https://doi.org/10.1002/cey2.65.

[193] Z. Pan, X. Ji, Facile synthesis of nitrogen and oxygen co-doped C@ Ti$_3$C$_2$ MXene for high performance symmetric supercapacitors, J. Power Sources. 439 (2019), 227068, https://doi.org/10.1016/j.jpowsour.2019.227068.

[194] H. Li, X. Wang, H. Li, S. Lin, B. Zhao, J. Dai, W. Song, X. Zhu, Y. Sun, Capacitance improvements of V$_4$C$_3$Tx by NH$_3$ annealing, J. Alloys Compd. 784 (2019) 923–930, https://doi.org/10.1016/j.jallcom.2019.01.111.

[195] Y.i. Tang, J. Zhu, W. Wu, C. Yang, W. Lv, F. Wang, Synthesis of nitrogen-doped two-dimensional Ti$_3$C$_2$ with enhanced electrochemical performance, J. Electrochem. Soc. 164 (4) (2017) A923–A929.

[196] Y. Wen, T.E. Rufford, X. Chen, N. Li, M. Lyu, L. Dai, L. Wang, Nitrogen-doped Ti$_3$C$_2$Tx MXene electrodes for high-performance supercapacitors, Nano Energy 38 (2017) 368–376, https://doi.org/10.1016/j.nanoen.2017.06.009.

[197] C. Yang, W. Que, Y.i. Tang, Y. Tian, X. Yin, Nitrogen and sulfur Co-doped 2D titanium carbides for enhanced electrochemical performance, J. Electrochem. Soc. 164 (9) (2017) A1939–A1945.

[198] C. Yang, W. Que, X. Yin, Y. Tian, Y. Yang, M. Que, Improved capacitance of nitrogen-doped delaminated two-dimensional titanium carbide by urea-assisted synthesis, Electrochim. Acta. 225 (2017) 416–424, https://doi.org/10.1016/j.electacta.2016.12.173.

[199] H. Niu, X. Yang, Q. Wang, X. Jing, K. Cheng, K. Zhu, K. Ye, G. Wang, D. Cao, J. Yan, Electrostatic self-assembly of MXene and edge-rich CoAl layered double hydroxide on molecular-scale with superhigh volumetric performances, J. Energy Chem. 46 (2020) 105–113, https://doi.org/10.1016/j.jechem.2019.10.023.

[200] X. Wang, H. Li, H. Li, S. Lin, J. Bai, J. Dai, C. Liang, X. Zhu, Y. Sun, S. Dou, Heterostructures of Ni–Co–Al layered double hydroxide assembled on V4C3 MXene for high-energy hybrid supercapacitors, J. Mater. Chem. A. 7 (2019) 2291–2300, https://doi.org/10.1039/C8TA11249E.

[201] Y. Zhao, J. Guo, A. Liu, T. Ma, 2D heterostructure comprised of Ni$_3$S$_2$/d-Ti$_3$C$_2$ supported on Ni foam as binder-free electrode for hybrid supercapacitor, J. Alloys Compd. 814 (2020), 152271, https://doi.org/10.1016/j.jallcom.2019.152271.

[202] X. Chen, S. Wang, J. Shi, X. Du, Q. Cheng, R. Xue, Q. Wang, M. Wang, L. Ruan, W. Zeng, Direct laser etching free-standing MXene-MoS$_2$ film for highly flexible micro-supercapacitor, Adv. Mater. Interfaces. 6 (2019) 1901160, https://doi.org/10.1002/admi.201901160.

[203] W. Hou, Y. Sun, Y. Zhang, T. Wang, L. Wu, Y. Du, W. Zhong, Mixed-dimensional heterostructure of few-layer MXene based vertical aligned MoS$_2$ nanosheets for enhanced supercapacitor performance, J. Alloys Compd. 859 (2021), 157797, https://doi.org/10.1016/j.jallcom.2020.157797.

[204] S. Xu, G. Wei, J. Li, W. Han, Y. Gogotsi, Flexible MXene–graphene electrodes with high volumetric capacitance for integrated co-cathode energy conversion/storage devices, J. Mater. Chem. A. 5 (2017) 17442–17451, https://doi.org/10.1039/C7TA05721K.

[205] Z. Fan, Y. Wang, Z. Xie, D. Wang, Y. Yuan, H. Kang, B. Su, Z. Cheng, Y. Liu, Modified MXene/holey graphene films for advanced supercapacitor electrodes with superior energy storage, Adv. Sci. 5 (2018) 1800750, https://doi.org/10.1002/advs.201800750.

[206] K. Nasrin, V. Sudharshan, K. Subramani, M. Karnan, M. Sathish, In-Situ synergistic 2D/2D MXene/BCN heterostructure for superlative energy density supercapacitor with super-long life, Small 18 (2022) 2106051, https://doi.org/10.1002/smll.202106051.

[207] H. Li, X. Li, J. Liang, Y. Chen, Hydrous RuO$_2$-decorated MXene coordinating with silver nanowire inks enabling fully printed micro-supercapacitors with extraordinary volumetric performance, Adv. Energy Mater. 9 (2019) 1803987, https://doi.org/10.1002/aenm.201803987.

[208] X. Zhang, S. Yang, W. Lu, D. Lei, Y. Tian, M. Guo, P. Mi, N. Qu, Y. Zhao, MXenes induced formation of Ni-MOF microbelts for high-performance supercapacitors, J. Colloid Interface Sci. 592 (2021) 95–102, https://doi.org/10.1016/j.jcis.2021.02.042.

[209] W. Liu, Z. Wang, Y. Su, Q. Li, Z. Zhao, F. Geng, Molecularly stacking manganese dioxide/titanium carbide sheets to produce highly flexible and conductive film electrodes with improved pseudocapacitive performances, Adv. Energy Mater. 7 (2017) 1602834, https://doi.org/10.1002/aenm.201602834.

[210] Y. Li, Y. Deng, X. Zhang, G. Ying, Z. Wang, J. Zhang, Facile fabrication of novel Ti$_3$C$_2$Tx-supported fallen leaf-like Bi$_2$S$_3$ nanopieces by a combined local-repulsion and macroscopic attraction strategy with enhanced symmetrical supercapacitor performance, Electrochim. Acta. 366 (2021) 137406, https://doi.org/10.1016/j.electacta.2020.137406.

[211] M. Boota, B. Anasori, C. Voigt, M.-Q. Zhao, M.W. Barsoum, Y. Gogotsi, Pseudocapacitive electrodes produced by oxidant-free polymerization of pyrrole between the layers of 2D titanium carbide (MXene), Adv. Mater. 28 (2016) 1517–1522, https://doi.org/10.1002/adma.201504705.

[212] W. Cheng, J. Fu, H. Hu, D. Ho, Interlayer structure engineering of MXene-based capacitor-type electrode for hybrid micro-supercapacitor toward battery-level energy density, Adv. Sci. 8 (2021) 2100775, https://doi.org/10.1002/advs.202100775.

[213] M. Zhu, Y. Huang, Q. Deng, J. Zhou, Z. Pei, Q.i. Xue, Y. Huang, Z. Wang, H. Li, Q. Huang, C. Zhi, others, Highly flexible, freestanding supercapacitor electrode with enhanced performance obtained by hybridizing polypyrrole chains with MXene, Adv. Energy Mater. 6 (21) (2016) 1600969, https://doi.org/10.1002/aenm.201600969.

[214] L. Li, F. Wang, J. Zhu, W. Wu, The facile synthesis of layered Ti$_2$C MXene/carbon nanotube composite paper with enhanced electrochemical properties, Dalt. Trans. 46 (2017) 14880–14887, https://doi.org/10.1039/C7DT02688A.

[215] J. Zheng, X. Pan, X. Huang, D. Xiong, Y. Shang, X. Li, N. Wang, W.-M. Lau, H. Y. Yang, Integrated NiCo-LDHs@ MXene/rGO aerogel: componential and structural engineering towards enhanced performance stability of hybrid supercapacitor, Chem. Eng. J. 396 (2020), 125197, https://doi.org/10.1016/j.cej.2020.125197.

[216] Y. Wang, H. Dou, J. Wang, B. Ding, Y. Xu, Z. Chang, X. Hao, Three-dimensional porous MXene/layered double hydroxide composite for high performance supercapacitors, J. Power Sources. 327 (2016) 221–228, https://doi.org/10.1016/j.jpowsour.2016.07.062.

[217] M.M. Baig, I.H. Gul, S.M. Baig, F. Shahzad, 2D MXenes: Synthesis, properties, and electrochemical energy storage for supercapacitors-A review, J. Electroanal. Chem. 904 (2022), 115920, https://doi.org/10.1016/j.jelechem.2021.115920.

[218] S.M. Hatam-Lee, A. Esfandiar, A. Rajabpour, Mechanical behaviors of titanium nitride and carbide MXenes: A molecular dynamics study, Appl. Surf. Sci. 566 (2021), 150633, https://doi.org/10.1016/j.apsusc.2021.150633.

Further reading

[43] P. Eklund, J. Rosen, P.O.Å. Persson, Layered ternary Mn+1AXn phases and their 2D derivative MXene: an overview from a thin-film perspective, J. Phys. D. Appl. Phys. 50 (11) (2017), 113001, https://doi.org/10.1088/1361-6463/aa57bc.

[44] H. Wang, Y. Wu, X. Yuan, G. Zeng, J. Zhou, X. Wang, J.W. Chew, Clay-inspired MXene-based electrochemical devices and photo-electrocatalyst: state-of-the-art progresses and challenges, Adv. Mater. 30 (2018) 1704561, https://doi.org/10.1002/adma.201704561.

[49] F.S.M. Yakin, M.F. Abdullah, S.A.M. Badaruddin, M.I. Syono, N. Soriadi, Surface modification and properties modulation of rGO film by short duration H2 and NH3 plasma treatment, Mater. Today Proc. 42 (2021) 2996–3001, https://doi.org/10.1016/j.matpr.2020.12.811.

[50] T. Kuila, S. Bose, A.K. Mishra, P. Khanra, N.H. Kim, J.H. Lee, Chemical functionalization of graphene and its applications, Prog. Mater. Sci. 57 (2012) 1061–1105, https://doi.org/10.1016/j.pmatsci.2012.03.002.

[56] P.O.Å. Persson, J. Rosen, Current state of the art on tailoring the MXene composition, structure, and surface chemistry, Curr. Opin. Solid State Mater. Sci. 23 (6) (2019), 100774, https://doi.org/10.1016/j.cossms.2019.100774.

[69] C. Peng, P. Wei, X. Chen, Y. Zhang, F. Zhu, Y. Cao, H. Wang, H. Yu, F. Peng, A hydrothermal etching route to synthesis of 2D MXene (Ti$_3$C$_2$, Nb$_2$C): Enhanced exfoliation and improved adsorption performance, Ceram. Int. 44 (2018) 18886–18893, https://doi.org/10.1016/j.ceramint.2018.07.124.

[70] S. Yuan, S.-Y. Pang, J. Hao, 2D transition metal dichalcogenides, carbides, nitrides, and their applications in supercapacitors and electrocatalytic hydrogen evolution reaction, Appl. Phys. Rev. 7 (2020) 21304, https://doi.org/10.1063/5.0005141.

[95] Q. Jiang, Y. Lei, H. Liang, K. Xi, C. Xia, H.N. Alshareef, Review of MXene electrochemical microsupercapacitors, Energy Storage Mater. 27 (2020) 78–95, https://doi.org/10.1016/j.ensm.2020.01.018.

[96] Y. Wei, P. Zhang, R.A. Soomro, Q. Zhu, B. Xu, Advances in the synthesis of 2D Mxenes, Adv. Mater. 33 (2021) 2103148, https://doi.org/10.1002/adma.202103148.

[123] H. Zhang, K. Dasbiswas, N.B. Ludwig, G. Han, B. Lee, S. Vaikuntanathan, D. V. Talapin, Stable colloids in molten inorganic salts, Nature 542 (2017) 328–331, https://doi.org/10.1038/nature21041.

[177] Q. Tang, Z. Zhou, P. Shen, Are MXenes promising anode materials for Li ion batteries? Computational studies on electronic properties and Li storage capability of Ti$_3$C$_2$ and Ti$_3$C$_2$X$_2$ (X= F, OH) monolayer, J. Am. Chem. Soc. 134 (2012) 16909–16916, https://doi.org/10.1021/ja308463r.